E.O. Paton Electric Welding Institute of the National Academy of Science of Ukraine
International Association “Welding”

# The Paton Welding Journal

07
2024

International Scientific-Technical and Production Journal ♦ Founded in January 2000 (12 Issues Per Year)



**Address of Editorial Office**
E.O. Paton Electric Welding Institute, 11 Kazymyr Malevych Str., 03150, Kyiv, Ukraine
Tel./Fax: (38044) 205 23 90, E-mail: journal@paton.kiev.ua, patonpublishinghouse@gmail.com
https://patonpublishinghouse.com/eng/journals/tpwj

The Journal was registered by the National Council of Ukraine on Television and Radio Broadcasting on 09.05.2024,
carrier identifier R30-04569; ISSN 0957-798X; DOI: http://dx.doi.org/10.37434/tpwj

**Subscriptions,** 12 issues per year:
$384 — annual subscription for the printed (hard copy) version, air postage and packaging included;
$312 — annual subscription for the electronic version (sending issues in pdf format or providing access to IP addresses).

**Representative Offices of “The Paton Welding Journal”:**

**BRAZIL, Arc Dynamics**
*Address*: Nova Iguacu, Rio de Janeiro, Brazil
Daniel Adolpho, Tel.: +55 21 9 6419 5703, E-mail: dadolpho@arcdynamics.com.br

**BULGARIA, Bulgarian Welding Society**
*Address*: Blvd. Asen Yordanov No.10, Sofia 1592, Bulgaria
Pavel Popgeorgiev, Tel.: +359 899 96 22 20, E-mail: office@bws-bg.org

**CHINA, China-Ukraine Institute of Welding, Guangdong Academy of Sciences**
*Address*: Room 210, No. 363 Changxing Road, Tianhe, Guangzhou, 510650, China
Zhang Yupeng, Tel.: +86-20-61086791, E-mail: patonjournal@gwi.gd.cn

**POLAND, PATON EUROPE Sp. z o. o.**
*Address*: ul. Kapitałowa 4, 35-213, Rzeszów, Poland
Anton Stepakhno, Tel.: +38067 509 95 67, E-mail: Anton.Stepakhno@paton.ua

The content of the Journal includes articles received from authors from around the world in the field of welding, cutting, cladding, soldering, brazing, coating, 3D additive technologies, electrometallurgy, material science, NDT and selectively includes translations into English of articles from the following journals, published in Ukrainian:

- Automatic Welding (https://patonpublishinghouse.com/eng/journals/as);
- Electrometallurgy Today (https://patonpublishinghouse.com/eng/journals/sem);
- Technical Diagnostics & Nondestructive Testing (https://patonpublishinghouse.com/eng/journals/tdnk).

# CONTENTS

## ORIGINAL ARTICLES

**D. Kovalchuk, L. Tretiakov, P.R. Carriere, Nanda Gopal Matavalam**
MANUFACTURING A CONSOLIDATED COPPER-STAINLESS STEEL BIMETALLIC PRODUCT USING xBEAM 3D METAL PRINTING ..... 3

**L. Chałko**
STRUCTURAL-PHASE CHARACTERISTICS OF DAMAGE TO WELDED JOINTS OF TPP STEAM PIPELINES FROM HEAT-RESISTANT STEELS (REVIEW)* ..... 10

**I.O. Ryabtsev, A.A. Babinets, I.P. Lentyugov, J. Niagaj, A. Czuprynski**
WELDING AND TECHNOLOGICAL PROPERTIES OF FLUX-CORED WIRE WITH THE CHARGE IN THE FORM OF GRANULATED POWDER** ..... 17

**V. Uchanin, G. Nardoni, P. Nardoni**
FATIGUE CRACKS DETECTION IN THE FILLET ZONE OF STEEL BLADES OF INDUSTRIAL GAS TURBINES USING EDDY CURRENT METHOD**** ..... 22

**V.M. Torop**
PRACTICE OF IMPLEMENTING THE METHODOLOGY OF RISK ANALYSIS OF THE OPERATION OF WELDED METAL STRUCTURES IN UKRAINE ..... 29

**M.M. Gasik**
OPTIMIZATION OF THE REFRACTORY LINING FOR FERROMANGANESE PRODUCTION FURNACE*** ..... 35

**D.V. Shevchenko, S.V. Prykhodko, A.A. Nadtochii, V.Yu. Shutov, A.M. Ovcharuk**
DEVELOPMENT OF THE TECHNOLOGY OF FERRONICKEL PRODUCTION IN UKRAINE*** ..... 39

FUTURE TRENDS AND TECHNOLOGIES IN THE WELDING INDUSTRY: VISION OF DNIPROMETYZ TAS ..... 46

*Translated Article(s) from «Avtomatychne Zvaryuvannya» (Automatic Welding), No. 3, 2024.

**Translated Article(s) from «Avtomatychne Zvaryuvannya» (Automatic Welding), No. 4, 2024.

***Translated Article(s) from «Suchasna Elektrometalurhiya» (Electrometallurgy Today), No. 2, 2024.

****Translated Article(s) from «Tekhnichna Diahnostyka ta Neruinivnyi Kontrol» (Technical Diagnostics & Nondestructive Testing), No. 2, 2024.

**Indexing:** The electronic edition of the Journal is stored in the V.I. Vernadsky National Library of Ukraine (eVerLib), included in the OPEN UKRAINIAN CITATION INDEX database and international databases: CROSSREF, EBSCO, Google Scholar, INDEX COPERNICUS, IET Inspec, ULRICHSWEB.

DOI: https://doi.org/10.37434/tpwj2024.07.01

# MANUFACTURING A CONSOLIDATED COPPER-STAINLESS STEEL BIMETALLIC PRODUCT USING xBeam 3D METAL PRINTING

**D. Kovalchuk[1], L. Tretiakov[1], P.R. Carriere[2], Nanda Gopal Matavalam[2]**

[1]JSC NVO Chervona Hvilya
28 Dubrovytska Str., 04200, Kyiv, Ukraine
[2]RadiaBeam Technologies, LLC
1717 Stewart Str., Santa Monica, CA 90404, USA

**ABSTRACT**

The creation of strong and tight copper and stainless steel joints in mechanical structures and components is an actual challenge in modern engineering. Thanks to unique combination of different properties such joints have many important applications like components of linear particle accelerators, ultra-high vacuum systems (up to $10^{-8}$ torr), heat exchangers, even of the international fusion experimental reactor. At the same time, ensuring a reliable joint of immiscible materials such as copper and stainless steel is a technologically challenging problem due to significantly different physical, mechanical and metallurgical properties, including melting points, thermal expansion coefficients, thermal conductivity, etc. Traditional approaches to the production of such joints, based on certain welding methods, impose many technical and geometric limitations due to the need for special preparation of the contact surfaces of the parts to be joined or the uncontrolled formation of new phases when mixing melts of different metals. As for brazing methods, they do not always provide reliable vacuum-tight joints for relatively thick parts and do not guarantee sufficient joint strength. Therefore, it is important to find more technologically flexible ways to solve such problems. This article discusses a new approach to joining copper and stainless steel using the xBeam 3D Metal Printing technology. This novel directed energy deposition (DED) technology uses a profile electron beam and coaxial feeding of copper wire to deposit it upon a precision machined stainless steel substrate. The results of the exploration study of joints made using this method are presented, including the study of vacuum tightness of the joint, density of the deposited material, metallurgy of the interface, electrical conductivity, oxygen content, hardness in different zones, etc. Specialized preheating strategies minimized the thermal deformation of the machined substrate, a key consideration for adding multimaterial functionality to monolith components.

**KEYWORDS:** copper, stainless steel, joining, bimetals, additive manufacturing, metal 3D printing, electron beam, DED-wire

## INTRODUCTION

Complex consolidated assemblies of different materials are used in various industries due to the ability to optimally combine the best mechanical, thermal and chemical properties in one product, which cannot be achieved by manufacturing from a single material. In particular, the bimetallic combination of copper and stainless steel is of great interest, as it creates a unique combination of excellent properties. Stainless steel combines high strength, satisfactory ductility, and low thermal conductivity, while copper has high thermal and electrical conductivity, high ductility, as well. Both materials have good corrosion resistance in various environments. Due to this combination of properties, consolidated copper and stainless steel bimetallic products are used in critical components of nuclear reactors, linear accelerators, ultrahigh-vacuum equipment, thin film deposition systems, heat exchangers, experimental physics environments, etc.

However, obtaining a reliable joint of copper and stainless steels is a technologically challenging task due to significantly different thermophysical, mechanical and metallurgical properties, such as melting point and heat of fusion, thermal expansion coefficients, thermal conductivity, viscosity, surface tension coefficients, etc. It is also worth considering that stainless steel is an alloy of Fe–Cr–Ni (along with a number of impurities such as C, Si, Mn, S, P and Cu), while copper is a pure metal element. This requires attention to physical and chemical aspects of the interaction between these materials when joining them.

Various methods of joining copper and stainless steel, both in the solid state and through melt contact, are known, including diffusion joining [1], various welding and brazing processes [2–5], and 3D printing processes using lasers or traditional thermionic electron beam guns as heating sources and consumables in the form of powder or wire [6–7]. However, each process has certain limitations and issues, so the task of developing new methods for creating bimetallic combinations of copper and stainless steel remains relevant.

## STATEMENT OF WORK

In this paper, the authors demonstrate a methodology for producing a consolidated product in the form

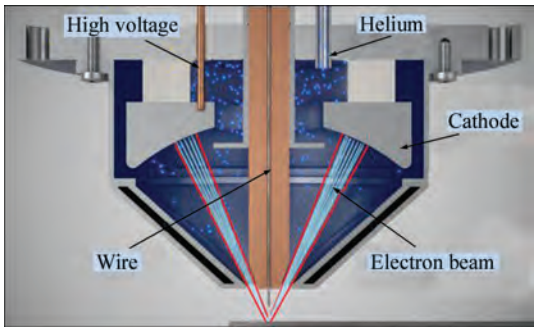


**Figure 1.** Formation of an electron beam in the form of a hollow inverted cone in xBeam 3D metal printing technology

of a thick-walled, high-purity copper cylinder tightly attached to a preprecision machined stainless steel flange (Conflat™) using xBeam metal 3D printing technology.

Conflat flanges are routinely in vacuum systems as part of demountable assembly method. Conflats are particular useful for achieving ultra-high vacuum, as they copper gasket enables higher bakeout temperatures than conventional polymeric gaskets while also providing a helium-impermeable barrier. The seal is formed via a knife edge machined into the stainless steel which plastically deforms, or bites, into the softer copper gasket. Unlike polymer o-rings sealing methods, the form and finish of a conflat knife edge must be much more precise. Flatness of the knife edge is critically important, as the shallow (0.5 mm) knife edge must uniformly engage with the copper gasket. The flatness and dimensions of the knife edge are therefore critical, as they must ensure perfectly uniform contact with the copper sealing gasket.

The xBeam metal 3D printing technology was chosen for this study due to the excellent control of thermal processes in and around the melt pool during the layer-by-layer formation of the deposited product, which allowed us to expect, firstly, the formation of a consolidated joint between two materials with different physical properties, and secondly, minimization of residual distortions of the machined substrate, since their processing after depositing the copper cylinder is not allowed.

The xBeam metal 3D printing technology uses a hollow conical profile electron beam as a heating source, which is directly generated by a gas discharge electron gun, and a wire is used as a feedstock for deposition, which is fed coaxially with the mentioned profile electron beam directly into the center of the deposition zone [8] (Figure 1). This configuration allows the same electron beam to create a melt pool on the substrate and simultaneously melt the feedstock wire above the melt pool, reducing the thermal impact on the substrate material and controlling the melt pool parameters well [9] (Figure 2) — this is especially important to avoid excessive mixing of the two different materials and the corresponding impact of the difference in their physical and chemical properties.

The moderate energy density of the low-voltage (<20 kV) electron beam and the dispersed edges of the beam focus significantly reduce the temperature gradients in the substrate material and the previously printed layers of the added material. This gradual temperature gradient reduces the thermally induced stress gradients, thus minimizing cracking, residual stresses and deformation [10].

## EXPERIMENT

The experiment was conducted on the xBeamLab laboratory 3D printing system.

Standard commercial conflates DN35-DN40 with an outer diameter of 69.85 mm (2.75″ OD) made of 304L stainless steel were used for the experiments (Figure 3). The metal-to-metal sealing edge of this conflate is made on an inner diameter of 41.91 mm (1.650″). These conflates were used as substrates for

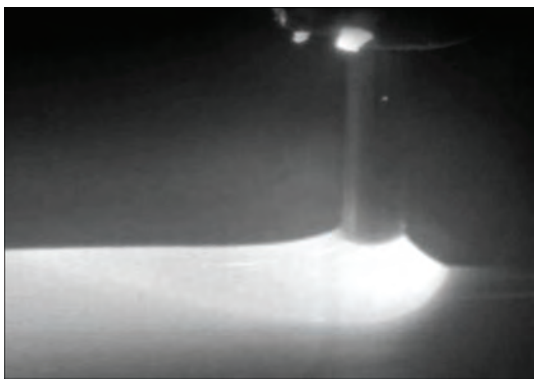

**Figure 2.** Photo of the actual deposition process using xBeam 3D metal printing technology

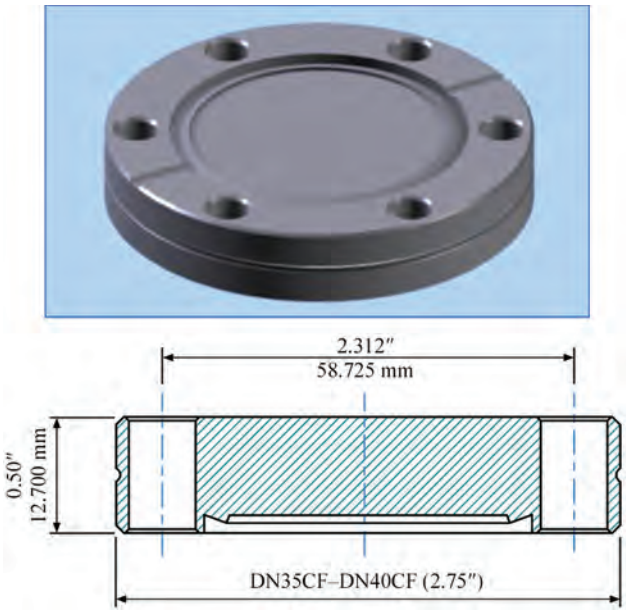


**Figure 3.** Stainless steel conflat

the deposition of pure copper wire with subsequent layer-by-layer build-up of copper cylinders using xBeam 3D metal printing technology. The final dimensions of the copper cylinders after finishing were set (Figure 4), accordingly, technologists determined the parameters of the model for 3D printing, taking into account allowances for processing. At the same time, any processing of conflates after the production of the consolidated product was not allowed.

A 2 mm diameter wire of pure copper grade M1 (Cu > 99.9 %, oxygen content no more than 20 ppm) was used as a feedstock for deposition. Since the oxygen content of copper is critical for high-vacuum applications, pure helium (99.995 %) was used as the working gas of the gas-discharge electron beam gun to minimize the absorption of oxygen from the residual atmosphere of the operating chamber.

Heating processes, i.e. turning on the electron beam gun, started at a vacuum of $5 \cdot 10^{-2}$ mbar. Then the residual pressure in the operating chamber was increased due to the supply of operating gas to the EB gun, and the technological 3D printing process was carried out at a partial pressure of helium of $3–5 \cdot 10^{-1}$ mbar.

The Conflat substrate was placed in cylindrical sockets made in a thick copper plate. Such a decision made it possible to carry out preliminary indirect heating of the conflates before deposition by means of heat conduction from a copper plate, which was slowly heated by an electron beam for a certain time. The gradual heating of the substrate stabilized the processing temperature and reduced the thermal gradients. Specifically, the heat deposited into the part from the molten copper is balanced against radiative heat loss into the surrounding processing chamber as well as conduction loss into the deposition fixture. By stabilizing these temperature profiles with a large, preheated thermal mass, the internal stresses in the body during printing is reduced.

After preliminary heating of the substrates (conflates), copper wire was deposited on them. On each

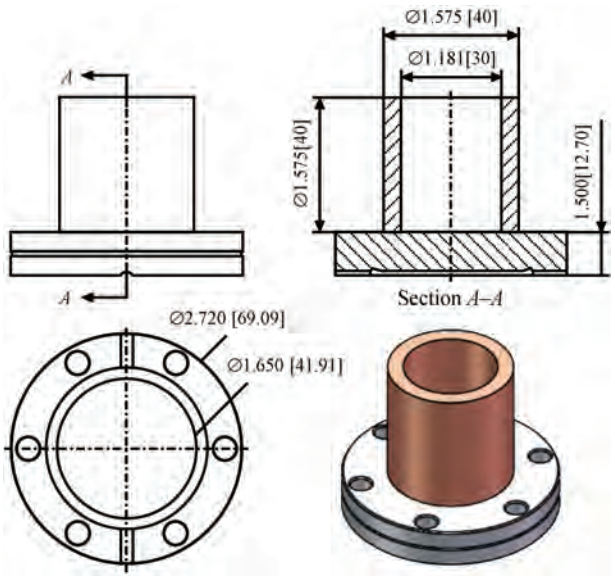


**Figure 4.** Dimensions of the final consolidated product

layer, the wire was deposited with two coaxial rings of different diameters to form the required thickness of the cylinder wall, taking into account the allowance for its finishing mechanical processing.

The thickness of the layer when forming the copper cylinder was 1.4 mm with a wire feed rate of 14 mm/s. The power of the electron beam was from 5 to 5.5 kW at an accelerating voltage of 18 kV while the deposition travel speed was set to 10mm/sec. This made it possible to deposit 2 mm copper wire with a net productivity of about 1.4 kg/h. To prevent excessive heat accumulation in the 3D printed material, pauses were used before starting to print the next layer. Considering all technological factors, the complete printing time of one consolidated product was about 40 minutes.

## INVESTIGATION OF SAMPLES AND DISCUSSION

As a result, four samples were produced, one of which (Figure 5) was used to conduct a number of exploratory studies, including metallographic analysis of the consolidation zone of the two materials, determina-

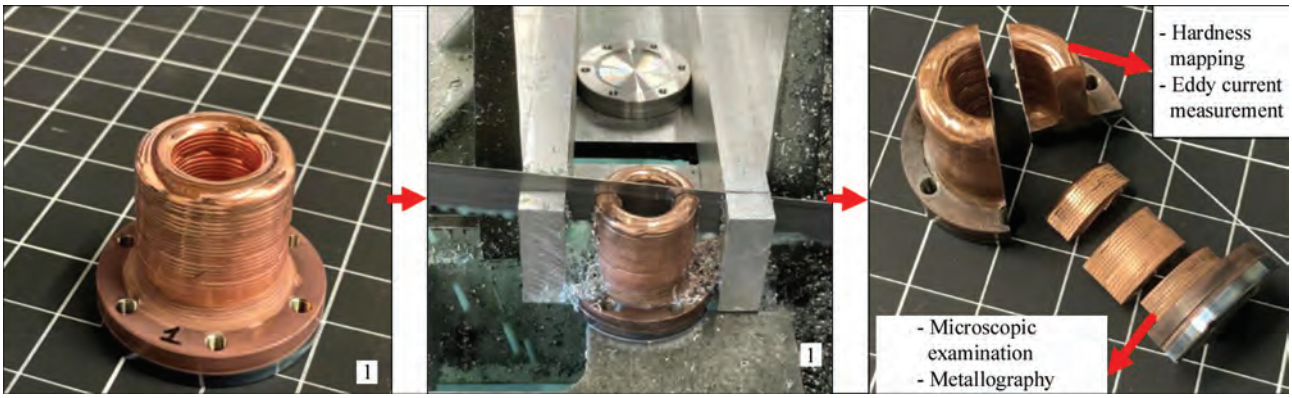


**Figure 5.** 3D printed consolidated product and sample cutting scheme for research (left) as deposited copper on substrate (center) bandsaw cutting of sample for analysis (right) sectioning of sample

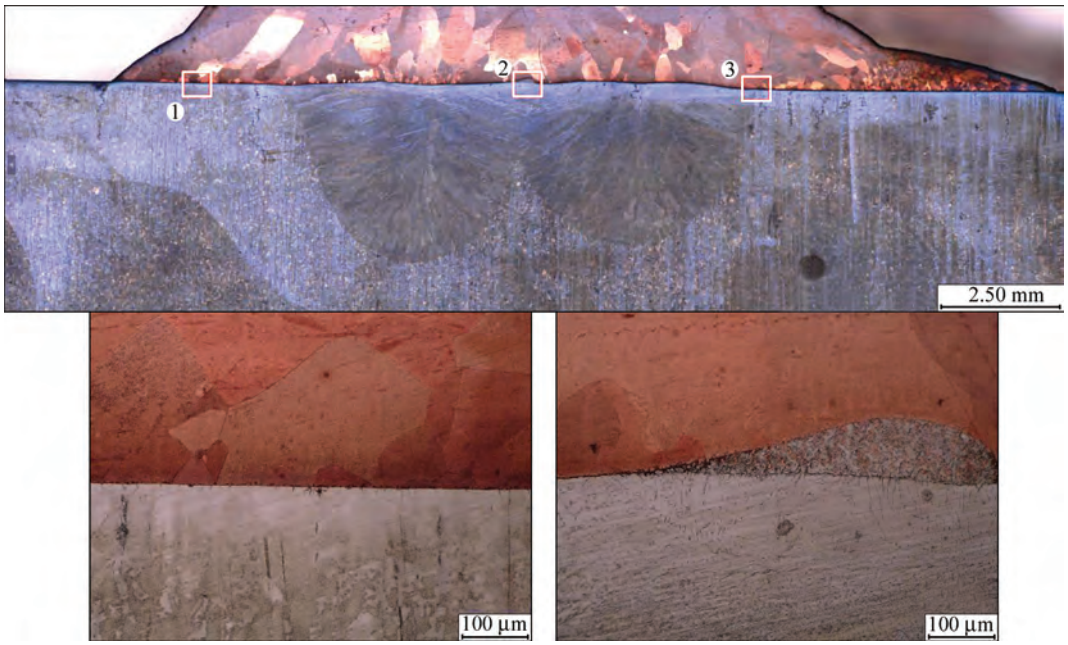


**Figure 6.** (Upper) Macrograph of etched copper/stainless steel interface demonstrating HAZ in stainless steel as well as variable grain size distribution in the substrate/copper interface. (Bottom-left) Micrograph of copper/substrate interface at region 1 highlighted above, demonstrating sharp boundary between copper and stainless. (Bottom-right) Micrograph of interface region 2, demonstrating copper infiltration into porous stainless steel bump above interface

tion of gas content, density, hardness, electrical conductivity of the 3D printed material, determination of the influence of the process deposition on the residual distortion of conflates, etc.

The electrical conductivity was evaluated using the eddy-current method at 480 kHz, according to ASTM E1004 by comparison with the electrical conductivity value in the traceable reference sample. The

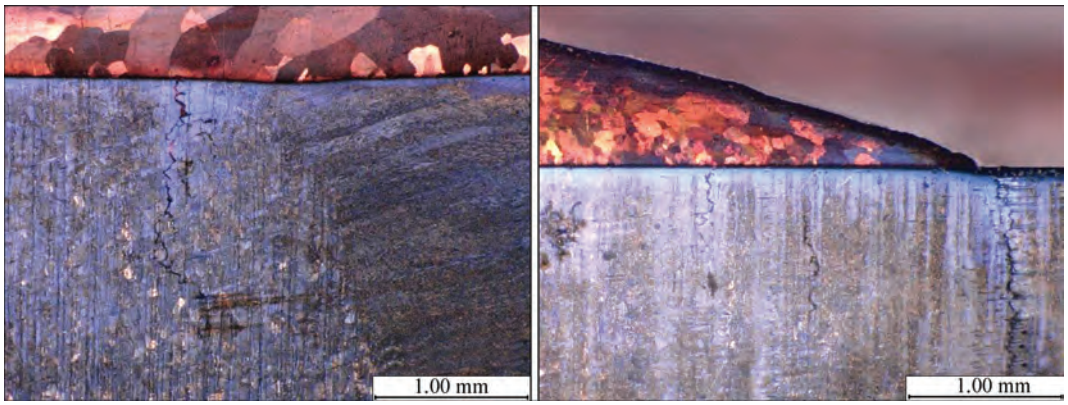


**Figure 7.** Micrographs of copper/stainless steel interface demonstrating large grain-boundary crack backfilled with copper (left); additional interface cracks at inner edge of deposit (right)

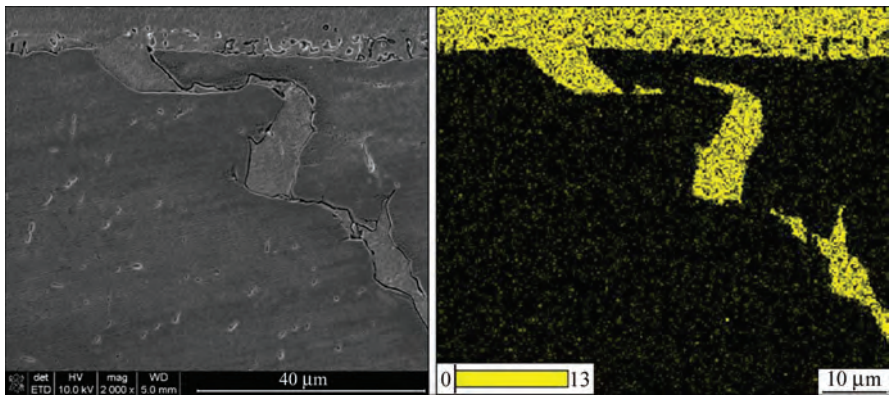


**Figure 8.** Deep penetration of copper into the stainless steel cracks

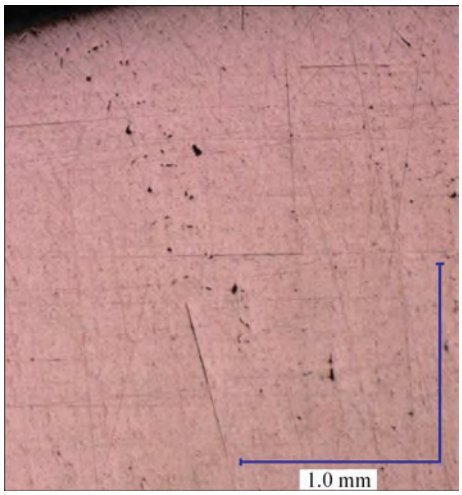


**Figure 9.** The pore detection area is 1000×1000 μm in size

electrical conductivity 3D printed pure copper was 99.2 (±0.4) % IACS of the reference value.

The oxygen content was measured on LECO equipment according to the requirements of ASTM E1019-18. As a result, the actual oxygen content of the wire used for deposition was 4 ppm, and the oxygen content of three samples cut from different areas of the 3D printed material was 2 ppm — that is, the vacuum 3D printing process provided a certain refinement of pure copper from oxygen, which has positive effect on properties.

Metallographic analysis of the consolidation zone of the two materials showed a dense and strong connection without the formation of new phases. A macrograph of the etched substrate/deposit interface is shown below in Figure 6 with the inner edge of the deposit on the left-hand size. This macrograph demonstrates a heat affected zone (HAZ) in the stainless steel from the first layer deposition, as well as a fine grain copper microstructure at the interface. The fine grain microstructure is especially evident on the

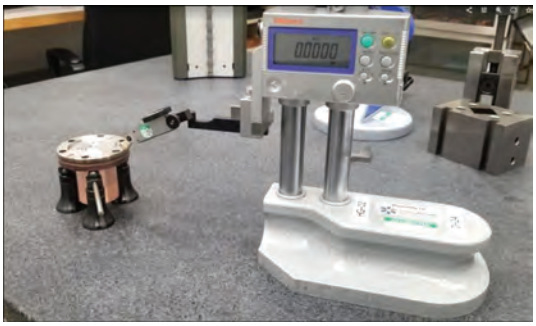

**Figure 11.** Flatness measurement

leftmost region of the copper deposit, as shown in Figure 7.

A significant number of cracks are observed at the copper/stainless steel interface, which are backfilled with copper, as shown in the micrographs of Figure 7.

Scanning electron microscopy with energy dispersive spectroscopy shows deep penetration of copper into the stainless steel crack (Figure 8).

The density of the 3D printed material was determined by calculating the total area of detected pores in three arbitrarily selected zones measuring 1000×1000 μm each (Keyence grain area analysis) using special software.

In this way, an approximate density of about 99.1 % was determined, which is probably explained by the presence of a large number of small pores ranging in size from units to tens of microns (Figure 9). The variety of shapes and sizes of pores indicate the different nature of their formation — from insufficient fusion of layers to the release of impurity vapors in closed zones during the melting process.

Vickers microhardness was performed at the triple point of the stainless steel fusion zone boundary and the copper deposit, which is region 3 of Figure 6 above. The hardness values show that the stainless steel retains its hardness after deposition of approxi-

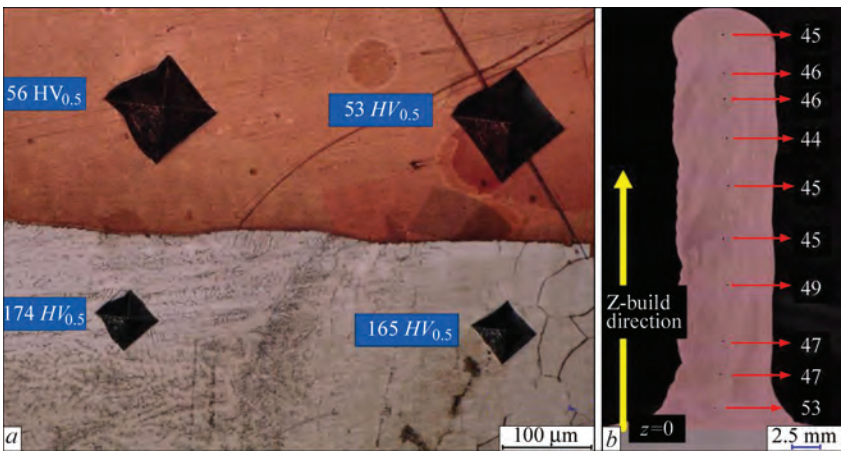


**Figure 10.** Determination of microhardness and its dependence on height: *a* — microhardness along the length of the deposit following direction of samples growth; *b* — Vickers microhardness at stainless steel fusion zone/base metal/copper interface, at location <3> of Figure 6; *c* — diagram of the dependence of microhardness on the distance from the substrate in the direction of sample growth


**Figure 12.** Measurement of the helium leakage of the conflate joint (*a*) and the contact surface between the deposited material (copper) and the substrate (stainless steel conflate) (*b*)

mately 165 *HV*, while the copper at the interface has a hardness of annealed, dead-soft copper.

The microhardness of the 3D printed copper was measured along the direction of sample growth (see Figure 10, *a*) as demonstrated in Figure 10, *b*. The obtained data presented in the diagram (Figure 10, *c*) show fairly uniform Vickers microhardness values with some tendency to decrease with distance from the substrate. This is probably related to the number of heating-cooling thermocycles, which decreases with increasing layer number, i.e. with height. Small deviations from the average values indicate the uniformity of the structure of the deposited material.

As already mentioned above, the ability to prevent or minimize residual distortions of the substrate (conflates) under the influence of thermal processes during the consolidation is almost the most important factor in assessing the suitability of the method of obtaining a consolidated joint of copper with a stainless steel conflate.

The flatness (evenness) of the conflate was checked on the side opposite to the 3D printed cylinder. The measurement was made using a calibrated digital indicator with an accuracy of 0.0025 mm (0.0001″) (Figure 11).

In the same way, the flatness of the reference conflat (without the 3D printed copper cylinder) was checked.

The flatness of the reference conflate was <0.0127 mm (0.0005″), and the flatness of the tested sample obtained by 3D printing using xBeam technology was 0.03 mm (0.0012″). That is, it was detected that the residual distortion caused by thermal processes appeared during 3D deposition, but the additional deviation from flatness due to such distortion was very small — no more than 0.0173 mm (0.0007″).

In order to assess how critical the influence of the identified conflate deformation is on the vacuum tightness of the conflate joint, helium leak rate was measured using a high-precision helium detector (Figure 12, *a*). Helium leakage through the contact surface between the deposited material (copper) and the substrate (stainless steel conflate) was also measured (Figure 12, *b*).

In both cases, the absence of any leakage (within the measurement error) was found, which proved the absolute vacuum tightness of both the consolidated copper-stainless steel bimetallic product and the conflate joint using this product. This tests also demonstrated that the deformation of the substrate enabled a hermetic UHV seal on the premachined knife edge.

## CONCLUSIONS

Exploratory studies of a consolidated copper-stainless steel bimetallic product formed by 3D printing of a thick-walled cylinder of high-purity copper onto a stainless steel conflate using xBeam 3D metal printing technology demonstrated the following:

- The technological process described above ensured the creation of a strong and absolutely vacuum tight joint of copper with stainless steel, which is confirmed by the absence of helium leakage through the contact surface between the two materials;
- The 3D printing process of formation of a thick-walled copper cylinder upon the substrate of a stainless steel conflate caused only a slight residual deformation of no more than 0.0173 mm (0.0007″), which did not affect the sealing properties of the conflated joint;
- The deposited material (pure copper) has excellent physical properties with no oxygen pickup, sufficient to ensure the functional properties of the consolidated bimetallic product for its intended use;
- xBeam 3D metal printing technology is a promising method of creating consolidated, dissimilar metal joints of materials with different thermophysical and physicochemical properties due to a number of characteristic parameters of the layer-by-layer deposition process, first of all, excellent control of metallurgical processes in and around the melt pool during deposition.

## REFERENCES

1. Gaurang R. Joshi et al. (2022) The joining of copper to stainless steel by solid-state welding processes: A Review. *Materials*, 15(**20**), 7234. DOI: https://doi.org/10.3390/ma15207234
2. Raghavendra S. Darji et al. (2021) Exploiting the challenges of copper to austenitic stainless steel bimetallic joining by gas tungsten arc welding: A fluid flow perspective. In: *Proc. of IOP Conf. on Materials Sci. and Eng.*, **1146**, 012011. DOI: https://doi.org/10.1088/1757-899X/1146/1/012011

3. Gu, X., Cui, Z., Gu, X., Shao, J. (2021) Wire-feeding laser-welding of copper/stainless steel using different filler metals. *Materials*, 14(**9**), 2122. DOI: https://doi.org/10.3390/ma14092122
4. Turna, M., Sahul, M., Ondruska, J., Lokaj, J. (2011) Electron beam welding of copper to stainless steel. In: *Proc. of Inter. DAAAM Symp., Vienna, Austria*. Ed. by B. Katalinic. Vol. 22, 833–834.
5. Sahul, M., Sahul, M., Turˇna, M., Zacková, P. (2014) Disk laser welding of copper to stainless steel. *Adv. Mater. Res.*, **1077**, 76–81. DOI: https://doi.org/10.4028/www.scientific.net/AMR.1077.76
6. Osipovich, Kseniya S. et al. (2020) Gradient transition zone structure in "steel–copper" sample produced by double wire-feed electron beam additive manufacturing. *J. of Materials Sci.*, **55**, 9258-9272. DOI: https://doi.org/10.1007/s10853-020-04549-y
7. Rock, Christopher et al. (2021) Characterization of copper & stainless steel interface produced by electron beam powder bed fusion. *Materials & Design*, **212**, 110278. DOI: https://doi.org/10.1016/j.matdes.2021.110278
8. Kovalchuk, D.V., Melnik, V.I., Melnik, I.V., Tugaj, B.A. (2017) New possibilities of additive manufacturing using xBeam 3D Metal Printing technology (Review). *The Paton Welding J.*, **12**, 16–22. DOI: https://doi.org/10.15407/tpwj2017.12.03
9. Kovalchuk, D., Ivasishin, O. (2019) Profile electron beam 3D metal printing. In: *Additive Manufacturing for the Aerospace Industry*, 213–233. DOI: https://doi.org/10.1016/B978-0-12-814062-8.00012-1
10. Makhnenko, O.V., Milenin, A.S., Velikoivanenko, E.A. et al. (2017) Modelling of temperature fields and stress-strain state of small 3D sample in its layer-by-layer forming. *The Paton Welding J.*, **3**, 7–14. DOI: https://doi.org/10.15407/tpwj2017.03.02

**ORCID**
D. Kovalchuk: 0000-0001-9016-097X,
P.R. Carriere: 0000-0002-4793-5239,
Nanda Gopal Matavalam: 0009-0005-0676-6394

**CONFLICT OF INTEREST**
The Authors declare no conflict of interest

**CORRESPONDING AUTHOR**
D. Kovalchuk
JSC NVO Chervona Hvilya
28 Dubrovytska Str., 04200, Kyiv, Ukraine.
E-mail: dmytro@xbeam3d.com

**SUGGESTED CITATION**
D. Kovalchuk, L. Tretiakov, P.R. Carriere, Nanda Gopal Matavalam (2024) Manufacturing a consolidated copper-stainless steel bimetallic product using xBeam 3D metal printing. *The Paton Welding J.*, **7**, 3–9.
DOI: https://doi.org/10.37434/tpwj2024.07.01

**JOURNAL HOME PAGE**
https://patonpublishinghouse.com/eng/journals/tpwj

Received: 31.01.2024
Received in revised form: 12.04.2024
Accepted: 29.07.2024

DOI: https://doi.org/10.37434/tpwj2024.07.02

# STRUCTURAL-PHASE CHARACTERISTICS OF DAMAGE TO WELDED JOINTS OF TPP STEAM PIPELINES FROM HEAT-RESISTANT STEELS (REVIEW)

**L. Chałko**

Casimir Pulaski Radom University
ul. Malczewskiego 29, room 124, 26-600, Radom, Poland

**ABSTRACT**

The paper considers the peculiarities of damage to welded joints of steam pipelines that have been operated for a long time (more than 280 thou h) under creep and fatigue conditions. It was established that the damage caused by creep and fatigue depends to a large extent on a structural-phase state of the metal of welded joints, which changes considerably during their long-term operation. With longer service life of welded joints, a ferrite-carbide mixture forms in their structure as one of the components. The presence of such a mixture contributes to acceleration of damage to welded joints. The dependence of formation of the ferrite-carbide mixture on the initial structure of welded joints was established, and recommendations were given for producing an initial structure with improved quality characteristics, which is advisable for increasing their reliability and service life.

**KEYWORDS:** steam pipelines, welded joints, heat-resistant steels, structure, damage, reliability, service life, pores, fatigue cracks

## INTRODUCTION

Welded joints of steam pipelines largely determine the level of reliability of power units at thermal power plants (TPP). First of all, these are welded joints of steam pipelines of live steam, hot intermediate superheating, as well as steam pipelines within boilers. The metal of welded joints is characterized by the presence of structural, chemical and mechanical inhomogeneities, which at their long-term operation under creep conditions significantly contributes to appearance of micro- and macrodefects. The presence of such defects is considered as respective damage to welded joints [1–4]. The structural inhomogeneity grows with an increase in the service life of welded joints, which leads to a decrease in the resistance of metal of welded joints to its deformation and damage.

It should be noted that curvilinear and bending sections of steam pipelines (bends) also refer to the most damaging. However, the features of damage to bends and welded joints are different, that determines an individual approach to their study [5]. The impact of the support and suspension system, condition of tees, rebars, as well as operating conditions of welded joints on damage also requires separate study.

It is advisable to use the equipment of TPP (including steam pipelines and their welded joints), whose life is 35–45 years, up to 60–65 years (about 350 thou h). Namely such an operation of aging TPP requires 3.0–3.5 times less costs than replacing them with the new ones. And, therefore, individual testing of metal of welded joints of steam pipelines is required, as one of the most damaging components of TPP power units.



## THE AIM OF THE WORK

is to analyze the features of the influence of a structural-phase state on damage to welded joints of steam pipelines, operating for more than 280 thou h under creep and fatigue conditions.

## FEATURES OF PROCEDURE AND RESEARCH METHODS

The metal of steam pipelines of 12Kh1MF and 15Kh1M1F steels, in particular their welded joints after operation under creep conditions for more than 280 thou h are exposed to gradual degradation. And therefore, to determine the reliability of operation of steam pipelines, as well as their residual life, it is advisable to carry out appropriate complex studies. Such studies should be conducted in cooperation with experienced specialists from TPP and power systems. To solve the research tasks, specimens for sections from operating steam pipelines should be cut out in places where their damage is the most probable. The study of such sections allows determining to a large extent the real structural-phase state of the metal of welded joints, as well as their operational properties [1–3, 6–9]. For research, methods of microstructural, electron microscopic and micro X-ray spectral analyses, as well as X-ray method, are used. The studies of the mechanisms of creep and fatigue cracks formation are carried out with the use of optical and electron microscopy [4–9]. By using photometry as well as by X-ray patterns, respectively, the quantitative compo-

sition and structure of $M_3C$, $M_7C_3$, $M_{23}C_6$, $Mo_2C$ and VC carbides are determined, their shape and appearance are summarized, which allows increasing the accuracy of determining the type of carbides. The use of optical microscopy allows determining the size of bainite, ferrite, sorbite, troostite and pearlite grains, as well as austenite grains. Creep and fatigue life tests are required to determine the reliability and life of welded joints.

For the theoretical and practical solution of the mentioned tasks, it is advisable to use the appropriate mathematical apparatus [10, 11] in relation to simulation of the temperature mode of the welding process. It is advisable to optimize the welding mode parameters by taking into account the obtained results, which will allow producing welded joints with increased quality indices of their initial structure [12, 13]. At the same time, simulation allows clarifying the features of the creep and fatigue process in the metal of welded joints by comparing the obtained results with the indices of their properties [8, 9, 13].

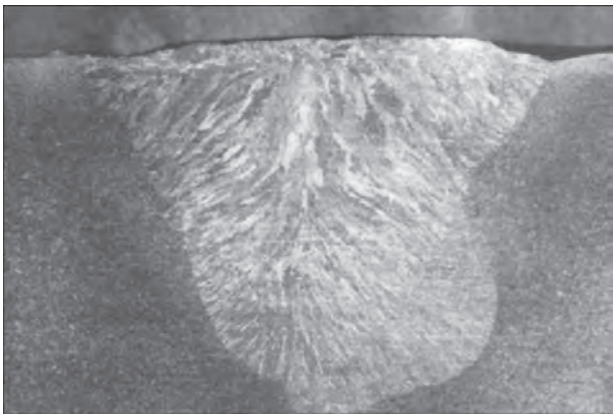

**Figure 1.** Macrostructure (×2.1) of welded joint of 15Kh1M1F steel

## RESULTS AND DISCUSSION

To produce operating steam pipelines, mostly 12Kh1MF and 15Kh1M1F steels were used. Steam pipelines, in which accordingly the largest damage after their operation for more than 280 thou h is observed, operate under normative recommended conditions: at a temperature of 545 °C and a pressure of 25.5 MPa. During operation of steam pipelines, their short-term overheating periods of up to 585 and even up to 600 °C are possible (emergency steam discharge).

The alloying elements like chromium, molybdenum and vanadium, included in the mentioned steels provide them appropriate physical and mechanical properties. The mentioned elements partially alloy

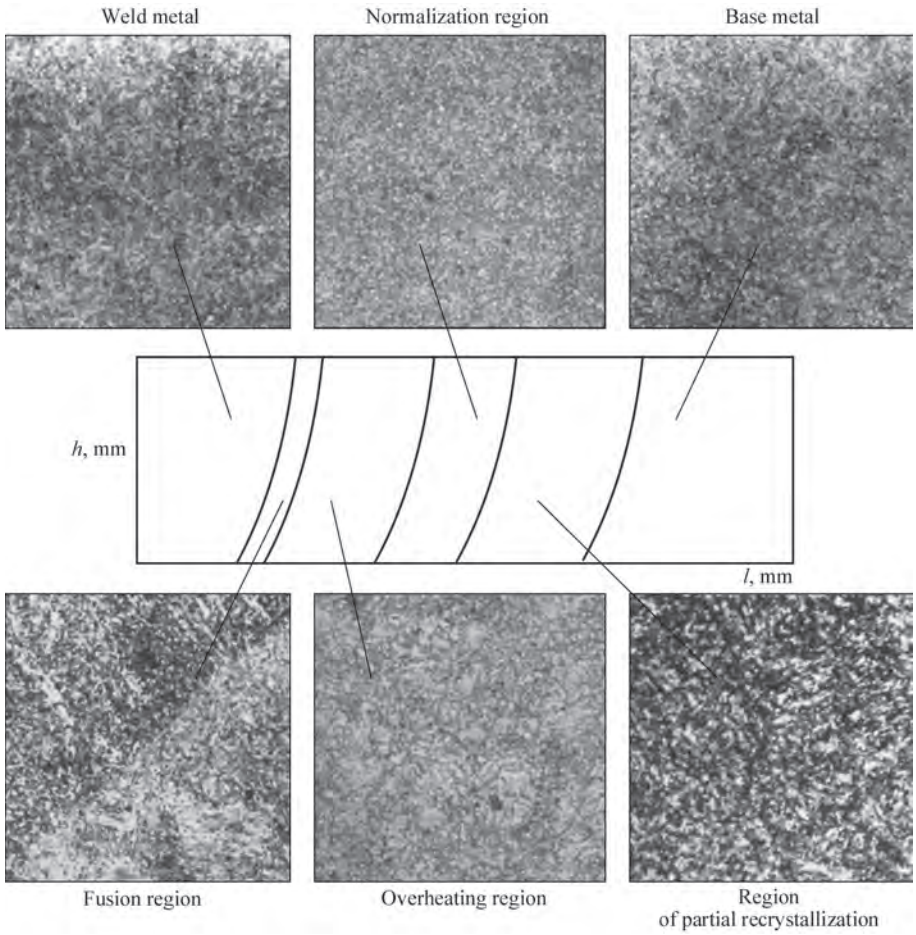


**Figure 2.** Microstructure (×100) of welded joint of 15Kh1M1F steel

**Table 1.** Chemical composition of 15Kh1M1F steel, wt.%

| C | Si | Mn | Cr | Mo | V | Ni | Cu | S | P |
|---|---|---|---|---|---|---|---|---|---|
| | | | | | | Not more than | | | |
| 0.10–0.16 | 0.17–0.37 | 0.40–0.70 | 1.10–1.40 | 0.90–1.10 | 0.20–0.35 | 0.25 | 0.25 | 0.025 | 0.025 |

**Table 2.** Chemical composition of electrode wire of Sv-09KhMFA grade, wt.%

| C | Si | Mn | Cr | Ni | Mo | V | S | P |
|---|---|---|---|---|---|---|---|---|
| 0.09 | 0.20 | 0.45 | 1.0 | 0.15 | 0.60 | 0.25 | 0.020 | 0.020 |

**Table 3.** Chemical composition of weld metal, wt.%

| C | Si | Mn | Cr | Mo | V | S | P |
|---|---|---|---|---|---|---|---|
| 0.09 | 0.15 | 0.30 | 1.0 | 0.60 | 0.21 | 0.019 | 0.019 |

α-phase grains (ferrite, tempering bainite, sorbite, troostite) and partially form the part of $M_3C$, $M_7C_3$, $M_{23}C_6$, VC and $Mo_2C$ carbides, providing dispersion strengthening of steels. Welded joints of 12Kh1MF and 15Kh1M1F steels are subjected to mandatory postweld tempering, which provides: strengthening of metal by precipitation of dispersed VC and $Mo_2C$ carbides in sufficient quantity; relief of welding stresses; substructural strengthening; thermal stability of the strengthened state; necessary service properties.

Macrostructure of welded joints is characterized by the presence of three characteristic regions, Figure 1: base metal, which did not undergo the effect of welding heating; weld metal; heat-affected zone.

Weld metal (Figure 2) represents a mixture of deposited electrode metal and partially molten base metal of a joint being produced.

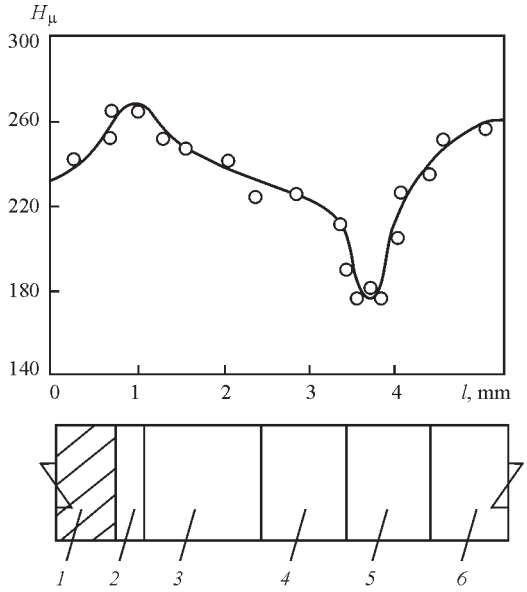


**Figure 3.** Microhardness of welded joint of 12Kh1M1F steel after operation of 290 thou h: *1* — weld metal; *2* — fusion region; *3* — overheating region; *4* — normalization region; *5* — region of partial recrystallization; *6* — base metal

The process of the molten metal crystallization begins from partially molten α-phase grains. The direction of crystal growth in the weld metal structure is coordinated with the heat removal. Welding on the optimized parameters of the mode of thick-walled steam pipes prevents the formation of relatively coarse ferrite grains in the regions of fusion and HAZ overheating (Figure 2) [10–12]. The formation of locally grouped liquation precipitations on side surfaces of crystals is also not admitted. At the same time, the formation of fine-grained, disoriented structure occurs (see Figure 2). On the macrosections (see Figure 1), the relief of each layer is clearly observed. Welding without preheating does not ensure the formation of the required amount of VC and $Mo_2C$ carbides in the weld metal, which promotes the reduction of its properties and leads to the acceleration of damage [1–4]. The chemical composition of the weld metal is different from the chemical composition of the base metal, for example, in mechanized welding in the $CO_2$ + Ar environment (respectively, 50 and 50 %) of steam pipelines of 15Kh1M1F steel (Table 1) with the use of the electrode wire of Sv-09KhMFA grade (Table 2), chemical composition of the weld metal (Table 3).

Heat-affected zone representes the area of the base metal (see Figure 2), in which under the effect of welding heating, the structure was formed, which is different from the structures of the base and weld metal. Accordingly, mechanical properties are also characterized by the presence of differences (Figure 3).

The width of HAZ of welded joints of steam pipelines amounts to about 4.3–5.4 mm and is clearly observed on the macro- and microsections. Such observation makes it possible to determine the presence of normatively not recommended structures in HAZ [1, 2], as well as the presence of structures of, for example, pearlite, in which at the service life of more than 280 thou h, accelerated damage is admitted.

The metal of the region of the HAZ fusion (see Figure 2) is heated in the temperature range $T_L$–$T_S$, its width in welded joints, produced using regulatory-recommended and optimal mode parameters, is 0.1–0.2 mm. In this region, diffusion processes actively occur, which at increased parameters of the mode promotes the possible formation of coarse austenitic and ferritic grains [3, 13].

The structure of the overheating region (see Figure 2) is formed under the effect of welding heating in the temperature range $T_L$ — 1150 °C (approximate). The width of the region amounts to 1.2–1.8 mm. At long-term exposure higher than $A_{c3}$, coarse austenitic grains (grain size number is 3–5, DSTU 8972:2019) can be formed in this region, which is observed in welded joints of thick-walled steam line pipes, for example, in steam pipelines of live steam (diameter is 630 mm, wall thickness is 60 mm).

The normalization region is subjected to welding heating in the temperature range of 1150 °C (approximate) — $A_{c3}$. Its width amounts to 0.9–1.1 mm. The structure of the region is fine-grained. The mechanical properties of the region are higher than similar properties of other HAZ regions, and damage is respectively lower.

The structure of the partial HAZ crystallization region (Figure 4) is formed under the influence of welding heating in the temperature range $A_{c1}$–$A_{c3}$. The width of the region is about 2.1–2.3 mm. Welding heating provides a partial formation of austenitic grains. A complete transformation α→γ does not occur. And respective to the cooling rate after welding, as a result of γ→α transformation, pearlite, sorbite or troostite can be formed, which generally enhances structural inhomogeneity. Pearlite component is especially undesirable, the presence of which contributes to the acceleration of the process of reforming the initial structure into a ferrite-carbide mixture. Such a process takes place at a long-term operation of welded joints under creep conditions.

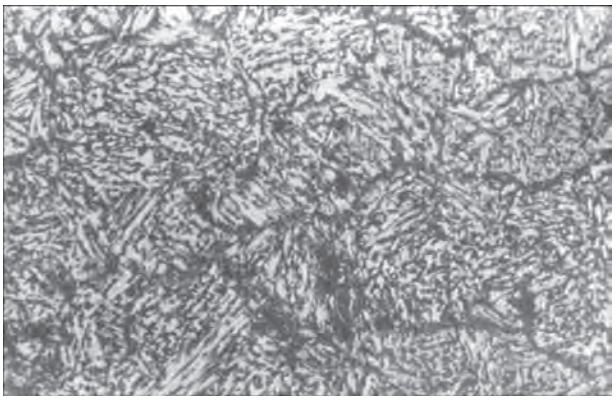

**Figure 4.** Microstructure (×300) of region of partial recrystallization of HAZ of welded joint of 15Kh1M1F steel [6]

Structural-phase transformations in the metal of welded joints, as a result of which a ferrite-carbide mixture is formed, depend to a large extent on their initial structure. The presence of such a mixture promotes the reduction in mechanical properties and an increase in damage to welded joints. For example, strength indices are reduced by 10–15 % and impact toughness by 15–20 % [8, 13]. Fatigue life and creep indices also depend on a structural-phase state of steels of steam pipelines. Thus, 12Kh1MF and 15X1M1F steels, having ferrite-bainite, ferrite-sorbite, ferrite-carbide and sorbite-troostite structures, are characterized by a spread of fatigue life of up to 37 % [1, 4, 8].

At a long-term operation of welded joints under creep and fatigue conditions, their damage, depending on a structural-phase state, grows significantly.

**Table 4.** Classification of damage to welded joints of 12Kh1MF and 15Kh1M1F steels with regard to their long-term operation under creep and fatigue conditions

| Metallographic feature | Damage area | Service life, thou h | Damage cause |
|---|---|---|---|
| Damage by creep and fatigue | | | |
| Stage I<br>Presence of pores along the grain boundaries, in places of grains contact with coagulating carbides, as well as on the body of grains | HAZ | > 250000 | Structural-phase, operational, technological, design |
| Stage II<br>Presence of pore chains along the grain boundaries, and pores on the body of grains | HAZ<br>Weld metal | > 280000 | Structural-phase, technological |
| Damage by fatigue | | | |
| Presence of fatigue-corrosion cracks having a grid and filamentous appearance | HAZ<br>Weld metal | > 270000 | Operational, structural-phase, technological |
| Fatigue transcrystalline cracks caused by cyclic mechanical loads under creep conditions | HAZ<br>Weld metal | > 280000 | Structural-phase, technological, operational |

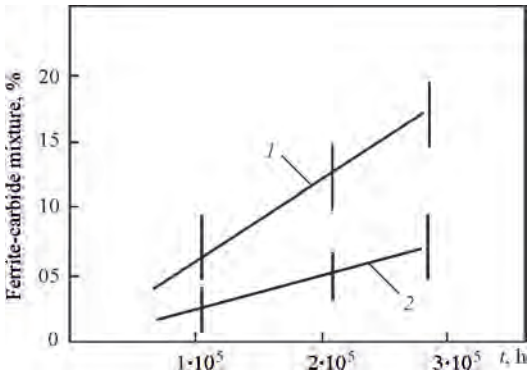


**Figure 5.** Dependence of ferrite-carbide mixture formation in the region of partial recrystallization of HAZ on the presence of structural components: *1* — recrystallized pearlite; *2* — sorbite. Welded joint of 15Kh1M1F steel

Therefore, it is advisable to classify the dependence of the growing damage on the features characterizing its formation (Table 4). The impact on the damage of design, technological and operational factors deserves a separate study [1–2, 4, 14–21].

Damage to welded joints by creep is featured by the predominant formation of pores on the grain boundaries in the places of the coagulating carbides contact with the α-phase grains. The mentioned damage mostly occurs in welded joints in the region of partial recrystallization of their HAZ, which is facilitated by the presence of pearlite components in its structure (see Figure 4). Namely this region is characterized by the largest softening among other regions, and its impact toughness is respectively lower.

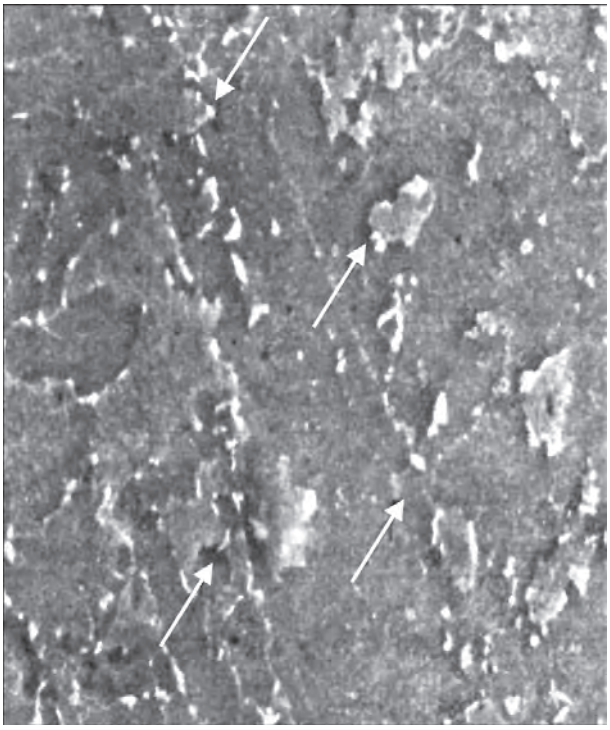

**Figure 6.** Embryonic creep micropores (arrows) in the metal of welded joint of 12Kh1MF steel. Service life is 280 thou h

Also, in the region of partial HAZ recrystallization, transformation of the initial structure into a ferrite-carbide mixture occurs at a higher rate (Figure 5).

In the metal of welded joints, which operate for a long time under conditions of creep transformation of the initial structure into a ferrite-carbide mixture, the following physicochemical processes are provided:

1. Self-diffusion of alloying elements and formation of segregations along the grain boundaries.
2. Coagulation of carbides, mostly $M_{23}C_6$.
3. Carbide reactions $M_3C \rightarrow M_7C_3 \rightarrow M_{23}C_6$.
4. Travel of dislocations by sliding and climbing, as well as accumulation and annihilation of dislocations.
5. Formation of vacancies, which by fusion are transformed into microdiscontinuities and further into embryonic pores (Figure 6). Pores grow in sizes, their quantity increases, and pores are transformed into creep cracks.

The mentioned processes depend largely on the initial structure of welded joints and, therefore, take place in the HAZ regions at different rates. For example, their rate in the region of partial recrystallization, due to the presence of recrystallized pearlite grains, is higher than in other HAZ regions (see Figure 4). The deformation of this region significantly exceeds the deformation of other HAZ regions, as well as weld and base metal [3, 8]. Accordingly, the damage to the metal of this region is greater (Figure 6). In the regions of fusion and overheating, in relation to the operation of welded joints for more than 280 thou h, the rate of these processes is also accelerated, which is associated with the presence of coarse austenitic grains and requires a separate study. In general, occurrence of the considered processes in the HAZ regions is more intensive than in the weld and base metal.

Formation of fatigue cracks under creep conditions in the metal of welded joints of steam pipelines and elements of their systems is caused by the action of variable stresses. Such cracks at operation of welded joints for more than 280 thou h are formed in the regions of design and technological stress concentrators, and namely near the backing rings of butt welded joints, in the places of contact of pipe elements of different thicknesses, from undercuts, lacks of fusion, crystallization cracks and other defects (Figure 7). During operation of welded joints for more than 280 thou h, the spectrum of their formation expands. For example, cracks start forming in the region of HAZ fusion of butt and fillet welded joints. In general, the propagation of fatigue cracks is caused by thermal fatigue, which is facilitated by thermal and corrosion components of this mechanism. The propagation of fatigue cracks is also contributed by physicochemical processes occurring under creep conditions. Thermal

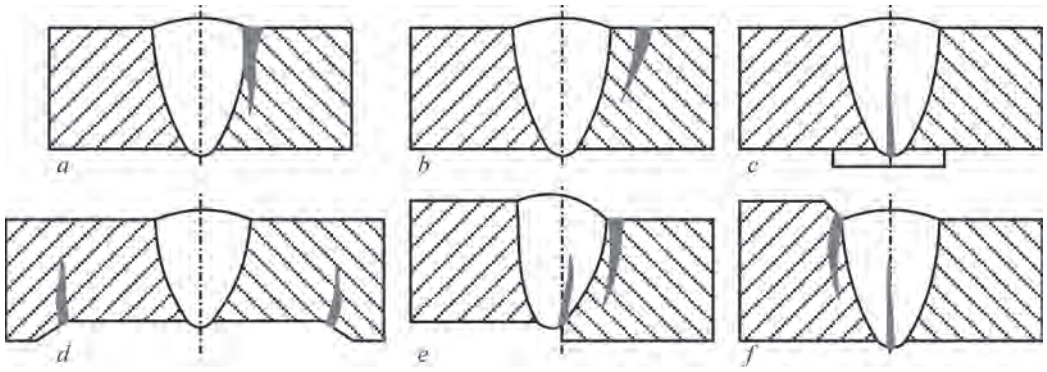


**Figure 7.** Typical damages of welded joints of steam pipelines: *a* — creep crack in the region of HAZ fusion; *b* — creep crack in the region of partial HAZ recrystallization; *c* — fatigue crack at the weld root near the backing ring; *d* — fatigue crack in the places of contact of pipe elements of different thicknesses; *e* — fatigue crack at displacement of steam pipeline pipes welded abutt; *f* — fatigue crack in welded joints of different thicknesses

fatigue leads to the formation of elongated cracks with probable branching. Depending on the structural state and thermal stresses, cracks may be single, as well as have the appearance of local grid cracking. Corrosion-fatigue cracks are mainly initiated on the inner surface of steam pipelines. Their propagation is facilitated by the presence of welding defects as well as defects of technological origin.

Fatigue cracks caused by cyclic mechanical loads are formed and start propagating from the outer surface of welded joints (see Figure 7). Such cracks are also formed in the contact places of pipe elements of different thicknesses.

According to the results of static analysis on the array of 50 welded joints, operated under creep conditions for more than 280 thou h, a total dependence of damage to their metal on the manifestation of the following factors was established: at a temperature rise to over 545 °C (e.g., emergency steam discharge), the damage is rapidly growing; the damage depends on a structural-phase state and the presence of initial defects. About 75–89 % of damages from its total amount occurs in the region of partial HAZ recrystallization (soft layer), as well as in the overheating region, where austenitic grains are coarse (size number is 3–5). The damage caused by the manifestation of initial defects, is about 20–25 % of its total amount.

To determine the reliability and residual life of welded joints of steam pipelines at their operation for more than 280 thou h, it is advisable to know the dynamics of the dependence of damage of their metal on the considered peculiarities.

## CONCLUSIONS

1. It was established that during operation of welded joints of steam pipelines for more than 280 thou h under creep conditions, their structural-phase state is mainly the main factor that leads to the damage of welded joints by creep.

2. It was determined, that producing welded joints of steam pipelines on the optimized mode parameters allows obtaining sorbite or troostite as recrystallization components in the region of partial HAZ recrystallization, and preventing the formation of pearlite.

3. Systematization of physico-chemical processes occuring in the metal of welded joints, operating for a long time under creep and fatigue conditions was proposed. The presence of such systematization is necessary for the study of features of individual processes, which is appropriate for the development of new steels.

4. It was found that the rate of formation of ferrite-carbide mixture in the structure of long-term operating welded joints depends on the presence of a pearlite component in their structure. The rate of formation of such a mixture can be reduced by producing welded joints with improved indices of their initial structure.

## REFERENCES

1. (2004) SOU-N MPE 40.1.17.401: *Metal control and extension of the service life of the main elements of boilers, turbines and pipelines of thermal power plants. Standard Instruction.* DonORGRES. Kyiv, OEP GRIFRE [in Ukrainian].
2. (2008) SOU-N EE 39.502: *Operation of pipelines of thermal power plants. Standard Instruction.* DonORGRES [in Ukrainian].
3. Dmytryk, V.V., Kasyanenko, I.V., Krakhmalyov, O.V. (2021) Structural-phase state and damage of welded joints of steam pipelines of thermal power plants. *Visnyk NTU KhPI. Series: Power and Thermotechnical Processes and Equipment,* 8(**4**), 56–63 [in Ukrainian]. DOI: https://doi.org/10.20998/2078-774X.2021.04.09
4. Banis, A., Duran, E.H., Bliznuk, V. et al. (2019) The effect of ultra-fast heating on the microstructure, grain size and texture evolution of a commercial low-C, medium-Mn DP steel. *Metals,* 9(**8**), 877. DOI: https://doi.org/10.3390/met9080877
5. Student, O., Krechkovska, G., Babii, L. (2013) Influence of heat changes during operation of steam pipelines of thermal power plants on static crack resistance of 15Kh1M1F steel. *Visnyk Ternopil. NTU,* 72(**4**), 199–206 [in Ukrainian].
6. Dmytryk, V.V., Garashchenko, O.S., Berdnikova, O.M. (2022) Determination of structural-phase state of welded

joints from pearlitic heat-resistant steels using the improved analysis method. *Avtomatych. Zvar.*, **6**, 11–16 [in Ukrainian]. DOI: https://doi.org/10.15407/as2022.06.02
7. Novotny, J., Honzikova, J., Pilous, V. et al. (2015) Properties of welded joints in power plant. *Manufacturing Technology*, 15(**6**), 1028–1032. DOI: https://doi.org/10.21062/ujep/x-.2015/a/1213-2489/MT/15/6/1028
8. Dmytryk, V.V., Kasyanenko, I.V., Latynin, Yu.M. (2021) Srtuctural state and damage of welded joint metal of steam pipelines. *Avtomatych. Zvar.*, **9**, 1–5 [in Ukrainian]. DOI: https://doi.org/10.15407/as2021.09.06
9. Dmitrik, V.V., Glushko, A.V., Grigorenko, S.G. (2016) Features of pore formation in welded joints of steam lines in long-term operation. *The Paton Welding J.*, **9**, 51–54. DOI: https://doi.org/10.15407/tpwj2016.09.11
10. Dmitrik, V.V., Kalinichenko, V.I. (2002) Numerical solutions of boundary problems of electric arc welding based on Galerkin scheme. *Dopovidi NANU*, **5**, 101–108 [in Russian].
11. Dmitrik, V.V., Glushko, A.V., Turenko, M.I. et al. (2018) Simulation of welding heating of produced power equipment joints. *Visnyk NTU KhPI. Series: Innovative technologies and equipment for treatment of materials in mechanical engineering and metallurgy*, 1318(**41**), 24–29 [in Ukrainian].
12. Dmitrik, V.V. (2000) Structure of welded joints from low-alloyed heat resistant Cr–Mo–V pearlitic steels. *The Paton Welding J.*, **4**, 27–30.
13. Glushko, A. (2016) Researching of welded steam pipe joints operated for a long time. *Eastern-European J. of Enterprise Technologies*, **6**, 84(**1**), 14–20. DOI: https://doi.org/10.15587/1729-4061.2016.85852
14. Kasatkin, O.G., Tsaryuk, A.K., Skulsky, V.Yu. et al. (2010) Peculiarities of technology of welding pipelines of dissimilar steels in nuclear power engineering. *The Paton Welding J.*, **1**, 35–37.
15. Skulsky, V.Yu., Tsaryuk, A.K., Gavrik, A.R. (2016) Selection of modes of high-temperature tempering of heat-resistant steel welded joints made by electrodes thermanit MTS616. *The Paton Welding J.*, **9**, 47–50. DOI: https://doi.org/10.15407/tpwj2016.09.10
16. Skulsky, V.Yu., Zhukov, V.V., Nimko, M.A. et al. (2016) Evaluation of susceptibility to temper brittleness of heat-resistant steels using high-temperature testing. *The Paton Welding J.*, **2**, 22–27. DOI: https://doi.org/10.15407/tpwg2016.02.04
17. Skulsky, V.Yu., Tsaryuk, A.K., Moravetsky, S.I. (2009) Evaluation of susceptibility of welded joints of heat-resistant chromium martensitic steel to cracking at heat treatment. *The Paton Welding J.*, **1**, 2–5.
18. Skulsky, V.Yu., Tsaryuk, A.K. (2004) New heat-resistant steels for manufacture of weldments in heat power units (Review). *The Paton Welding J.*, **4**, 35–40.
19. Skulsky, V.Yu. (2006) Features of δ-ferrite formation on the fusion boundary in welding heat-resistant chromium martensitic steel. *The Paton Welding J.*, **11**, 13–16.
20. Tsaryuk, A.K. (1999) Welding of heating surface of power boiler furnaces (Review). *Avtomatich. Svarka*, **1**, 34–40 [in Russian].
21. Gevorkyan, E., Prikhna, T., Vovk, R. et al. (2021) Sintered nanocomposites $ZrO_2$–WC obtained with field assisted hot pressing. *Composite Structures*, **259**. DOI: https://doi.org/10.1016/j.compstruct.2020.113443

**ORCID**
L. Chałko: 0000-0002-6179-109

**CORRESPONDING AUTHOR**
L. Chałko
Casimir Pulaski Radom University
ul. Malczewskiego 29, room 124, 26-600,
Radom, Poland.
E-mail: Leszek.chalko@uthrad.pl

**SUGGESTED CITATION**
L. Chałko (2024) Structural-phase characteristics of damage to welded joints of TPP steam pipelines from heat-resistant steels (Review). *The Paton Welding J.*, **7**, 10–16.
DOI: https://doi.org/10.37434/tpwj2024.07.02

**JOURNAL HOME PAGE**
https://patonpublishinghouse.com/eng/journals/tpwj

Received: 01.03.2024
Received in revised form: 08.05.2024
Accepted: 30.07.2024

DOI: https://doi.org/10.37434/tpwj2024.07.03

# WELDING AND TECHNOLOGICAL PROPERTIES OF FLUX-CORED WIRE WITH THE CHARGE IN THE FORM OF GRANULATED POWDER

**I.O. Ryabtsev**[1], **A.A. Babinets**[1], **I.P. Lentyugov**[1], **J. Niagaj**[2], **A. Czuprynski**[3]

[1] E.O. Paton Electric Welding Institute of the NASU
11 Kazymyr Malevych Str., 03150, Kyiv, Ukraine
[2]Upper Silesian Institute of Technology, Poland
[3]Silesian Polytechnic Institute, Poland

**ABSTRACT**

Comparative experimental studies have been carried out on the influence of the type and particle size distribution of the original metal granulated materials, which were used as a flux-cored wire charge, on its welding and technological properties during submerged arc surfacing. High-speed steel powder PG-R6M5 with 50–300 μm and 200–250 μm granulation, obtained by spraying of a melt metal, was used as a charge for experimental wires. The standard was flux-cored wire, the charge of which consists of ferroalloys with 50–300 μm granulation, calculated to ensure a similar chemical composition of the deposited metal and manufactured using standard technology. It has been experimentally determined that the welding and technological properties of three types of wires are at a high level, while the surfacing process with flux-cored wires, the charge of which contains granulated powder PG-R6M5, is characterized by greater stability, which results in an increase in melting and surfacing coefficients, and a decrease in the loss coefficient, compared to analogue wire with a charge of ferroalloy powders. It was also determined that the content of harmful impurities in the sample deposited with experimental wires with a charge of granulated powders is lower than in the standard sample. The patterns noted above indicate that the use of granulated powder in a flux-cored wire charge is not only technically feasible, but also leads to an increase in flux-cored wire homogeneity, which has a positive effect on their welding and technological properties.

**KEYWORDS:** arc surfacing, flux-cored wire, flux-cored wire charge, particle size distribution of powders, ferroalloys, welding and technological properties, deposited metal, surfacing stability, metallurgical heredity

## INTRODUCTION

It is widely known that service properties of surfaced parts are determined, primarily by the chemical composition and structure of the deposited layer metal, so that the method of complex alloying of the latter is usually used for their improvement [1–7]. At present, however, the technical and economic capabilities of such an approach have practically been exhausted. In addition, deposited metal alloying for the majority of surfacing processes, is performed through electrode and filler materials, in the charge of which mostly ferroalloys are mainly used, which are rather considerably contaminated by unwanted impurities.

The content of undesirable and even harmful impurities in the ferroalloys can be 2–5 times higher than in pure metal powders. For instance, the volume fraction of impurities in ferromanganese can be up to 0.4 %, in ferrotitanium — 0.6 %, in ferrosilicon ——1.0 %. One of the main contaminants in ferroalloys is sulphur, the content of which in high-carbon ferrochrome is equal to 0.08 %; in ferrotitanium it is up to 0.1%; in ferromolybdenum and ferrotungsten — up to 0.2 %. Here, the content of impurities is much lower in the powders of pure metals and alloys, manufactured by metal melt spraying. In particular, in the granulated powder of PG-R6M5 grade sulphur content is not higher than 0.03 % [8–10].

The majority of unwanted impurities in arc spraying pass into the deposited metal, thus causing certain negative metallurgical heredity, and they can impair the mechanical and service properties of the deposited metal. In this connection, at surfacing or welding there exist many chemical and technological methods of dealing with the impurities to improve the welding and technological properties of flux-cored wires and service properties of metal deposited using them [11–13].

In works [14–16] it is shown that application of granulated materials of certain types, produced by metal melt spraying, as flux-cored wire charge allows obtaining more uniform filling of the flux-cored wire and improving the arc process stability and, consequently, improving the quality of deposited metal formation and lowering the impurity content, which has a positive effect on its service properties.

## THE OBJECTIVE

of the work consists in a comparative study of the influence of the type and particle size distribution of granulated powders from high-speed steel R5M5 which were used as charge of flux-cored electrode wires instead of a composition from ferroalloys, on

its welding and technological properties and quality of deposited metal formation at electric arc surfacing.

## INVESTIGATION MATERIALS AND PROCEDURES

Three batches of experimental flux-cored electrode wires were produced with charge composition of three different types, which provide deposited metal of the same chemical composition of tool low-alloyed steel 30V2KhMF. For this purpose, the composition of the respective wires was calculated, in which the fill coefficient was ~ 30 %, and diameter was ~ 2.0 mm. Wire design is tubular with edge overlapping.

Granulated powder of PG-R6M5 grade was selected as charge for wire No. 1, with standard granulation of 50–300 μm. The same powder was used in the charge of wire No. 2. However, its particle size distribution was limited to narrower boundaries of 200–250 μm. Also the composition of wire No. 3 was calculated and it was manufactured. This wire could ensure production of deposited metal of chemical composition similar to that of wires Nos 1 and 2, but its charge consisted of ferroalloys of a standard granulation of 50–300 μm [11]. Determination and limitation of particle size distribution of the powders was performed using sieve analysis.

Deposition was performed by the automatic arc method under a layer of AN-26 flux in the same modes: wire feed rate of 120 m/h; that corresponded to current of ~200 A, voltage of 30 V, deposition rate of 18 m/h. The samples were first preheated up to the temperature of 280–300 °C to avoid hot cracks.

In order to avoid the influence of deposited metal mixing with the base metal (S235 to EN 10025-2) deposition of each sample was performed in five layers. Determination of the chemical composition, performed by the spectral method, and of hardness of the metal was conducted in the fifth deposited layer of each sample after its grinding.

Welding and technological properties of experimental wires were assessed by the following parameters:

- arc excitation pattern (easy, medium, complicated);
- stable arc burning (stable, satisfactory, unstable);
- deposited bead formation quality (sound, satisfactory, unsound);
- quality of slag crust detachment (easy, satisfactory, complicated);
- type and availability of defects in the deposited metal (absent, isolated, considerable number);
- melting characteristics (coefficients of melting, surfacing, and loss).

In order to calculate the coefficients of melting ($\alpha_m$), surfacing ($\alpha_d$) and losses for burnout and spatter ($\psi$), the weight of the plates and wires was determined before deposition and after it, and the deposition time was recorded. The respective coefficients were determined, using well-known expressions:

$$\alpha_m = G_m/(It); \quad (1)$$

$$\alpha_d = G_d/(It); \quad (2)$$

$$\psi = ((\alpha_m - \alpha_d)/\alpha_m)\cdot 100\ \%, \quad (3)$$

where $G_m$ is the molten metal weight, g; $G_d$ is the deposited metal weight, g; $I$ is the welding current, A; $t$ is the deposition time, h.

In addition to visual assessment, evaluation of arc process stability was performed by analyzing the integral values, which determine its energy state, such as for instance, arc voltage and current at their multiple recording [17]. In keeping with the procedure, the deviations of the values of arc current and voltage from average current value were analyzed by the calculated coefficients of variation. During the deposition process the mode parameters were analyzed using digital recoding multimeter ANENG AN9002, fitted with high-velocity analog-digital converter.

## INVESTIGATION RESULTS AND THEIR DISCUSSION

Visually, the metal deposited with all the types of experimental wires, has equally high quality of formation, no defects, and the quality of the slag crust detachment is satisfactory (Figure 1). The results of spectral analysis and measurement of the deposited metal hardness showed (Table 1) that the metal deposited with experimental wires of the three types, practically the same chemical composition and hard-

**Table 1.** Chemical composition and hardness of metal, deposited with experimental wires

| Number | Chemical composition of elements in the deposited metal, % | | | | | | | | | Hardness, *HRC* |
|---|---|---|---|---|---|---|---|---|---|---|
| | C | Cr | Mo | W | V | Mn | Si | S | P | |
| 1 | 0.19 | 1.2 | 1.64 | 1.70 | 0.50 | 0.3 | 0.56 | 0.020 | 0.022 | 30–32 |
| 2 | 0.19 | 1.2 | 1.71 | 1.74 | 0.51 | 0.3 | 0.56 | 0.021 | 0.024 | 29–31 |
| 3 | 0.25 | 1.38 | 1.27 | 1.63 | 0.35 | 0.38 | 0.73 | 0.027 | 0.037 | 28–32 |
| * | 0.2–0.3 | 1.0–1.4 | 1.0–1.7 | 1.5–2.0 | 0.3–0.5 | 0.3–0.5 | 0.3–0.5 | ≤0.04 | ≤0.04 | 30–35 |

*Calculated composition and deposited metal hardness.

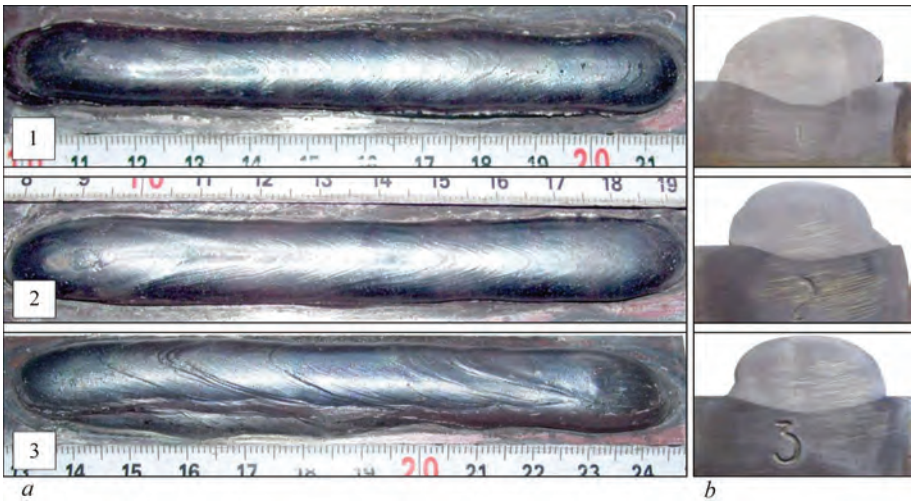


**Figure 1.** Appearance of samples deposited with wires Nos 1–3 in five layers (*a*), and their transverse macrosections (*b*)

**Table 2.** Comparative evaluation of welding-technological properties of experimental wires

| Parameter | Wire type | | |
|---|---|---|---|
| | No. 1 | No. 2 | No. 3 |
| Arc excitation pattern | Light | | |
| Arc burning stability | Stable | | |
| Quality of deposited bead formation | Sound | | |
| Quality of slag crust separation | Satisfactory | | |
| Presence of visible defects (pores, cracks, lacks-of-penetration, etc.) | None | | |
| Coefficients of, %:<br>● melting $\alpha_m$<br>● deposition $\alpha_d$<br>● losses $\psi$ | <br>17.1<br>16.8<br>1.75 | <br>16.2<br>15.8<br>2.47 | <br>13.6<br>12.6<br>7.35 |

**Table 3.** Comparative evaluation of the stability of the process of arc surfacing with experimental wires

| Parameter | Wire grade | | |
|---|---|---|---|
| | No. 1 | No. 2 | No. 3 |
| Set voltage, V | 28.0 | | |
| Minimal voltage, V | 26.03 | 25.91 | 25.27 |
| Maximal voltage V | 32.39 | 32.72 | 36.41 |
| Average voltage, V | 29.45 | 29.19 | 29.46 |
| Range of deviation by voltage, V | –1.97/+1.45 | –2.09/+4.72 | –2.73/+8.41 |
| Coefficient of arc voltage variation, | 4.72 | 4.99 | 6.07 |
| Set current, A | 200.0 | | |
| Minimal current, A | 136.4 | 127.8 | 128.6 |
| Maximal current, A | 252.0 | 266.0 | 312.0 |
| Average current, A | 194.8 | 194.9 | 214.6 |
| Range of current deviation, A | –63.6/+52.0 | –72.2/+66.0 | –71.4/+112.0 |
| Coefficient of voltage variation $K_I$, % | 14.12 | 14.71 | 16.18 |

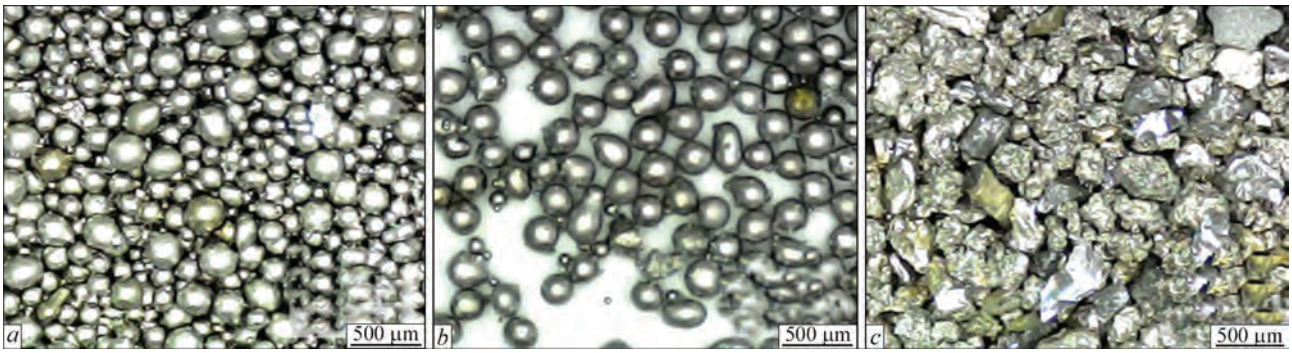


**Figure 2.** Appearance of samples of charge from powder R6M5 of 50 μm (*a*) and 200–250 (*b*) granulation, as well as from ferroalloys of 50–300 μm granulation (*c*)

ness, thus ensuring production of deposited metal of the type of low-alloyed tool steel 30V2KhMD. Note, the somewhat smaller, compared to the charge from ferroalloys, contamination by sulphur and phosphorus of the metal deposited using wires with charge from pure metal powders. This is attributable to lower content of these elements in the powders of high-speed steel R6M5.

Comparative evaluation of welding and technological properties of experimental wires (Table 2) showed that they are at approximately same level. However, wires Nos 1 and 2 with the charge, consisting of granulated powder of PG-R6M5 grade, have 1.2–1.3 higher coefficients of melting and surfacing, compared to the analogue wire with the charge from ferroalloys. In the same way, wires Nos 1 and 2 have 2.9–4.2 times lower coefficient of losses at deposition, compared to analogue wire.

Analysis of the data on current and voltage, obtained during surfacing with experimental wires showed (Table 3) that the most stable is the process of surfacing with wire No. 1: it is characterized by the smallest range of value deviation from average current and voltage. The process of surfacing with analogue wire No. 3 with a ferroalloy charge, is characterized by the lowest stability, which, apparently, is attributable to the fact that the kinetics of the process of melting of flux-cored wire, which contains components of the same composition and type (PG-R6M5 granulated powder), and also having identical physical properties (density, melting temperature, electric conductivity, etc.) will be characterized by higher stability, compared to melting kinetics of the wire, the charge of which contains ferroalloys and other components, for which these characteristics are different [18].

Somewhat higher welding-technological properties of wire No. 1, compared to wire No. 2 (both having charge from R6M5 granulated powder) can be accounted for, in our opinion, by the difference in the particle size distribution of the used powders. In wire No. 1 powders, consisting of globular particles of 50–300 μm size were used, and wire No. 2 had the same particles, but of 200–250 μm (Figure 2).

It is obvious that at application of components of the same, rather large size (200–250 μm) for the wire charge, voids form between the components during manufacture, which may affect the kinetics of flux-cored electrode wire melting. At application of powders with a wide range of particle size distribution from 50 to 300 μm in the charge, a much smaller number of such voids form in the charge, that is related to a higher density and homogeneity of the flux-cored wire, which melts in a more stable manner.

## CONCLUSIONS

1. A comprehensive comparative study of welding and technological properties of flux-cored wires for arc surfacing, in the charge of which materials of two different types — granulated powders and ferroalloys — were used, demonstrated that application of granulated materials in the flux-cored wire charge provides higher welding and technological properties, improvement of stability of arc surfacing process, quality of deposited metal formation and lowering of the content of sulphur and phosphorus impurities in them.

2. It was experimentally determined that the type of the initial charge components and their particle size distribution have a significant influence on the stability of arc surfacing process running, and, hence, they can affect the structure and service properties of the deposited metal.

## REFERENCES

1. Bely, A.I., Zhudra, A.P., Dzykovich, V.I. (2002) Effect of alloying elements on structure of composite alloy based on tungsten carbides. *The Paton Welding J.*, **11**, 17–19.
2. Ryabtsev, I.A., Senchenkov, I.K. (2013) *Theory and practice of surfacing works*. Kyiv, Ekotekhnologiya [in Russian].
3. Ryabtsev, I., Fomichov, S., Kuznetsov, V. et al. (2023) *Surfacing and additive technologies in welded fabrication*. Switzerland, Springer Nature AG.
4. Guk, V.A. (2000) Materials and technology for surfacing of machine parts operating under conditions of impact-abrasive wear. *The Paton Welding J.*, **8**, 11–13.

5. Skulsky, V.Yu. (2006) Effect of the degree of alloying of heat-resistant chromium steels on hardness of metal within the welded joint zone. *The Paton Welding J.*, **9**, 17–20.
6. Czupryński, A. (2020) Comparison of properties of hardfaced layers made by a metal-core-covered tubular electrode with a special chemical composition. *Materials*, 23(**13**), 5445. DOI: https://doi.org/10.3390/ma13235445.
7. Niagaj, J. (2011) Effect of niobium on properties of hardfaced layers surface welded by Fe–Cr–C open arc flux-cored wire electrodes. *Przegląd Spawalnictwa*, **10**, 67–72.
8. Gasik, M., Dashevskii, V., Bizhanov, A. (2020) *Ferroalloys: Theory and practice*. Switzerland, Springer Nature.
9. Kucher, I.G., Ol'shanskiy, V.I., Filippov, I.I., Kucher, I.I. (2020) *Ferroalloy manufacturer's handbook*, L'viv, Novyy Svit [in Russian].
10. Popov, V.S., Bilonik, I.M., Berezhny, S.P. (2003) Application of charge materials obtained by electroslag smelting to improve the quality of weld metal. In: *Abstr. of Papers on Modern Problems of Welding and Structural Life*. Kyiv, PWI, 60–61 [in Russian].
11. Pokhodnya, I.K., Suptel, A.M., Shlepakov, V.N. (1972) *Welding with flux-cored wire*. Kyiv, Naukova Dumka [in Russian].
12. Shlepakov, V.N., Naumejko, S.M. (2009) Peculiarities of desulphurisation of weld metal in flux-cored wire welding. *The Paton Welding J.*, **2**, 16–18.
13. Lentyugov, I.P., Ryabtsev, I.A. (2015) Structure and properties of metal deposited by flux-cored wire with charge of used metal-abrasive wastes. *The Paton Welding J.*, **6**, 87–89. DOI: https://doi.org/10.15407/tpwj2015.06.19
14. Kondratyev, I.A. (2015) *Flux-cored wire filled with granular alloy. Surfacing. Technologies, materials, equipment*: Coll. of Articles. Kyiv, PWI, 53–54 [in Russian].
15. Zhudra, A.P., Krivchikov, S.Yu., Dzykovich, V.I. (2014) Application of complex-alloyed powders produced by thermocentrifugal sputtering in flux-cored wires. *The Paton Welding J.*, **12**, 36–40. DOI: https://doi.org/10.15407/tpwj2014.12.08
16. Górka, J., Czupryński, A., Żuk, M. et al. (2018) Properties and structure of deposited nanocrystalline coatings in relation to selected construction materials resistant to abrasive wear. *Materials*, 11(**7**), 1184. DOI: https://doi.org/10.3390/ma11071184
17. Pokhodnya, I.K., Gorpenyuk, V.N., Milichenko, S.S. et al. (1990) *Metallurgy of arc welding: Processes in the arc and melting of electrodes*. Ed. by I.K. Pokhodnya. Kyiv, Naukova Dumka [in Russian].

## ORCID
I.O. Ryabtsev: 0000-0001-7180-7782
A.A. Babinets: 0000-0003-4432-8879,
I.P. Lentyugov: 0000-0001-8474-6819,
J. Niagaj: 0009-0001-6831-1548,
A. Czuprynski: 0000-0001-9337-8325

## CONFLICT OF INTEREST
The Authors declare no conflict of interest

## CORRESPONDING AUTHOR
A.A. Babinets
E.O. Paton Electric Welding Institute of the NASU
11 Kazymyr Malevych Str., 03150, Kyiv, Ukraine.
E-mail: a_babinets@ukr.net

## SUGGESTED CITATION
I.O. Ryabtsev, A.A. Babinets, I.P. Lentyugov, J. Niagaj, A. Czuprynski (2024) Welding and technological properties of flux-cored wire with the charge in the form of granulated powder. *The Paton Welding J.*, **7**, 17–21.
DOI: https://doi.org/10.37434/tpwj2024.07.03

## JOURNAL HOME PAGE
https://patonpublishinghouse.com/eng/journals/tpwj

Received: 16.04.2024
Received in revised form: 23.05.2024
Accepted: 18.07.2024

DOI: https://doi.org/10.37434/tpwj2024.07.04

# FATIGUE CRACKS DETECTION IN THE FILLET ZONE OF STEEL BLADES OF INDUSTRIAL GAS TURBINES USING EDDY CURRENT METHOD

**V. Uchanin**[1], **G. Nardoni**[2], **P. Nardoni**[2]

[1]G.V. Karpenko Physico-Mechanical Institute of the NASU
5 Naukova Str., 79060, Lviv, Ukraine
[2]I&T Nardoni Institute, Via della Cascina Pontevica, 21, 25124, Brescia, Italy

**ABSTRACT**

The results of experimental investigations aimed at the development of an effective eddy current technique for detection of fatigue cracks originated in the critical fillet zone of gas turbine blades fabricated of ferromagnetic steels are discussed. The proposed inspection technique is based on the use of selective eddy current probes (ECP) of double-differential type, providing high sensitivity when the clearance between the ECP operational surface and the inspected surface in the fillet zone is changed during the scanning. The experimental investigations signals from ECP of MDF 0501 type (operational surface diameter — 5 mm) allowed minimizing the lift-off effect by selecting the optimal operational frequency and choosing the optimal scanning parameters of the inspected zone. The effectiveness of the proposed inspection technique was confirmed with the application of a real gas turbine blade with the 2 mm long and 0.2 mm deep artificial defect in the fillet zone, which characterizes the sensitivity threshold specified in accordance with the technical assignment. The inspection technique has also been successfully used during its tests at enterprises of power engineering.

**KEYWORDS:** gas turbine blade, fillet zone, eddy current ECP, operational frequency

## INTRODUCTION

Gas turbine is called a blade machine, in which the potential energy of compressed and/or heated gas is converted into mechanical operation on the shaft. Its main elements are rotor with operating blades fixed on the discs, and stator. The design of a blade consists of airfoil, platform and shank. Blade airfoil is a metal profiled blade that directly contacts a working gas. Platform is the end airfoil section designed to reduce the vibration and protect the rim of a disc from the action of a heated gas. Shank serves to attach blades in the slot of a disc. Blades are the most critical parts of turbines operating under the conditions of cyclic and thermal stresses in combination with the corrosion and erosion processes under the action of a heated working gas. Gas turbines and their elements are the subject of constant modernization [1, 2]. The most rigid requirements for the quality, reliability and life are specified to blades of gas turbines, as many serious incidents during the operation of gas turbines are associated with their failure. Due to the critical concentration of stresses, researchers pay a particular attention to a fillet zone, where the coupling of a profiled airfoil with the platform surface of a blade is close to rectangular (Figure 1) [3]. Fractographic examinations showed that the main cause of failure of a gas turbine blade is multicycle fatigue [4, 5]. Primary crack can arise due to large inclusions of another phase [3] or corrosion phenomena [5, 6]. Failure and tearing of rotor blade fragments during operation can be a cause of the most serious accident because of significant damages to other turbine units. The economic aspect is also of great importance, which is associated with a high-cost fabrication of a blade unit, which can reach 35 % of a turbine cost as a whole.

**Figure 1.** Typical gas turbine compressor blade with an electro-erosion slot of 4 mm long, 0.2 mm deep and opening of 0.1 mm in the fillet zone for adjustment and checking of the inspection technique

The safe operation of gas turbines is guaranteed by a timely detection of operational defects by means of non-destructive inspection (NDI). Therefore, the development of effective methods of NDI of gas turbine blades is an urgent task of modern engineering.

## STATE OF THE PROBLEM

Periodic in-service NDI of blades and other gas turbine units is important for safe operation due to timely detection of defects before a complete failure of a structure. It is necessary to carry out NDI quickly and efficiently to minimize the shutdown period of a turbine. There are many NDI methods that can be used to check gas turbine components [6–8]. The method of penetrating liquids (colour method) using dye is a cost-effective NDI technique and simple in implementation, which is often used for NDI of gas turbine components. The drawbacks of this method are high requirements for the quality of surface cleaning and restrictions during NDI of corroded surfaces. Another restriction of this method is its suitability to detect only open cracks. Therefore, this method cannot be used for NDI of blades with protective coatings. The magnetic powder method allows detecting cracks in blades fabricated of ferromagnetic steels and is relatively low-cost. But it has the same restrictions as the method of penetrating liquids. The ultrasonic method can be used for NDI of blades [8]. But it also has disadvantages associated with the need in using contact liquids, which significantly complicates NDI in real industrial conditions of power engineering.

Considering the abovementioned, from our point of view, the most suitable method for in-service NDI of gas turbine blades is eddy-current NDI method [9–12]. But also during attempts to apply eddy-current NDI of blades, challenges arise, in particular related to:

1) a complex shape of a blade;

2) presence of clearances between the ECP during inspection of concave zones;

3) increased lift-off level characteristic of eddy-current NDI of products fabricated of ferromagnetic steels due to magnetic inhomogeneity of the material.

The most important thing when developing the eddy-current NDI technique for blades is to consider the complex shape of a blade (Figure 1) with curved convex and concave surfaces, edge and fillet zones, that are usually allocated as separate inspection zones, flaw detection of which is carried out after appropriate adjustment with taking into account the features of the specified zone.

Eddy-current NDI of zones with a large curvature radius at a remoted distance from the edge is not a cause for great concern and requires only manufacturing of special nozzles to orient the ECP perpendicular to the inspected surface. The problem of eddy-current NDI of the edge zones can be also solved by using appropriate nozzles that allow scanning the edge zone at a constant distance from the edge of a blade. When developing the procedure for blades inspection, the edge zone should be allocated to a separate zone, whose inspection requires balancing of the ECP, installing it at a certain distance from the edge with the appropriate adjustment of the eddy-current flaw detector (ECFD). Significant problems arise during the inspection of fillet zones between the platform and the airfoil of a blade, where fatigue cracks are most often formed during operation, which are mainly oriented along the fillet zone. These circumstances are the reasons for the development of special eddy-current inspection techniques built on using ECP of a complex shape, whose working surface reproduces the profile of an inspected surface in the fillet zone [13]. This approach limits the possibility of inspecting areas of a testing object (TO) with a different radius of surface curvature. ECPs on a flexible lining with a wide inspection zone are more versatile, but they do not meet the requirements for sensitivity to defects. To reduce the lift-off level characteristic of ferromagnetic steels when detecting cracks under the coating, pulsed eddy-current inspection method is promising [14–16]. Summarizing, we should note that this approach eliminates the possibility of using widespread ECFDs with harmonic excitation current, and serial ECFDs with a pulsed excitation are still absent at the market of eddy-current NDI means.

As noted above, the reliable detection of cracks in TO of ferromagnetic steels by the eddy-current method often interfere with the lift-off, induced from the magnetic and structural inhomogeneity of the material under study [12, 17, 18]. Therefore, in many outdated documents and publications, the eddy-current NDI method was determined as completely unsuitable or low-reliable for detecting defects in ferromagnetic steels. Let us note several approaches to reducing the effect of the mentioned specific lift-off. The first one consists in the additional magnetization of the TO area under study. This approach often gives a positive result, especially when introducing special screens in the ECP design (for example, Uchanin V.M. Eddy-current attachable probe for inspection of ferromagnetic materials. Patent of Ukraine No. 99379). However, additional screens increase the size of the ECP, which is not always appropriate. Moreover, additional magnetization limits the sensitivity of the ECP due to the magnetization of the ferrite core.

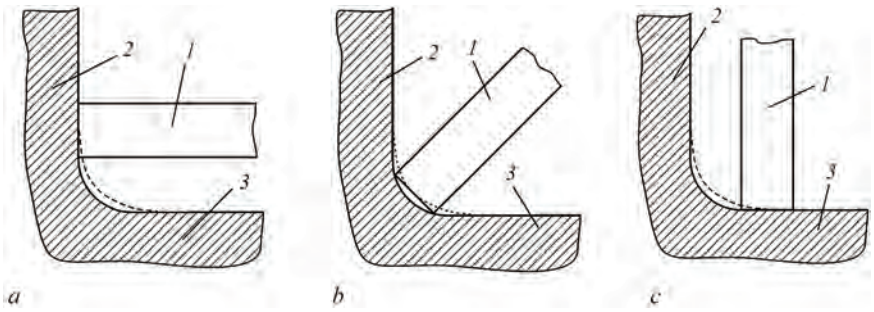


**Figure 2.** Location of ECP in the extreme position on the blade airfoil (*a*), in the zone of the maximum curvature of the fillet zone (*b*) and in the extreme position on the blade platform (*c*): *1* — ECP; *2* — blade airfoil; *3* — blade platform

Another approach can be implemented by creating selective ECPs, that have a low level of lift-off associated with the magnetic inhomogeneity of the TO material. Our experience shows that many complex problems of eddy-current detection of TO of ferromagnetic steel can be solved by using a double differential ECPs [17–20], which are composed of two generator and two measuring windings located at the square corners. All windings are wound on identical cylindrical ferritic cores. At the same time, both generator windings are connected in series and oriented to generate the same and opposite primary electromagnetic fields. Such a ECP design allows placing windings in a metal cylindrical case (usually from aluminium alloy), which significantly reduces the level of electronic lift-off. During wiring, the windings are thoroughly balanced, focusing on the minimum level of lift-off, which are formed as the ECP distance to a metal specimen in the form of a plane plate grows. When installing the windings in the metal case, it is necessary to provide an equal distance of the windings to the inner wall, so as not to violate the balance obtained during adjustment of the ECP.

**Figure 3.** Experimental mock-up of ECP of MDF 0501 type

## STUDYING THE ECP SIGNALS AND OPTIMIZATION OF INSPECTION MODES FOR FILLET ZONES OF BLADES

During transverse scanning of the fillet zone of a blade when using ECP of a cylindrical shape with a plane working surface, changes in the ECP distance from the TO surface occur, as it is schematically shown in Figure 2. Therefore, when choosing ECP, the preference should be given to ECPs of smaller diameter that are best adhere to the fillet surface. Previous studies have shown that to inspect fillet zones of a blade, ECPs of MDF 0501 type with an outer working diameter of 5 mm are best suited (Figure 3). In our case, such a small size of ECP allows scanning the fillet zone of a blade without creating clearances of more than 0.5 mm.

Signals from the ECP of MDF 0501 type were studied with the use of a standard specimen (SS) of SOP 2353.08 type (manufacturer — Promprylad, Kyiv) made of ferromagnetic 45 steel with electro-erosion defects of the type of a crack of different depth. Only defects of 0.2 and 0.5 mm deep were used for our research. The width (opening) of artificial defects is about 0.1 mm. The studies of sensitivity and registration of signals of the ECP were conducted by means of the eddy-current plate of EDDYMAX type of the Test Maschinen Technik Company, Germany. The scanning of the defective zone of the SS was performed at the optimal ECP orientation, when the line joining the excitation winding centers is oriented at an angle of 45° relative to the crack direction [20]. The signal from a crack has a "quasi-absolute" nature, when the maximum amplitude corresponds to the ECP position directly above the crack similarly to the ECP signal of an absolute type [20]. To choose the optimal orientation, on the ECP case, a special mark is applied (Figure 3).

The practical purpose of the experimental research is to choose the optimal frequency that will provide the best conditions for detecting defects in a convex fillet zone of a blade. The complex concept of such optimization involves the choice of opera-

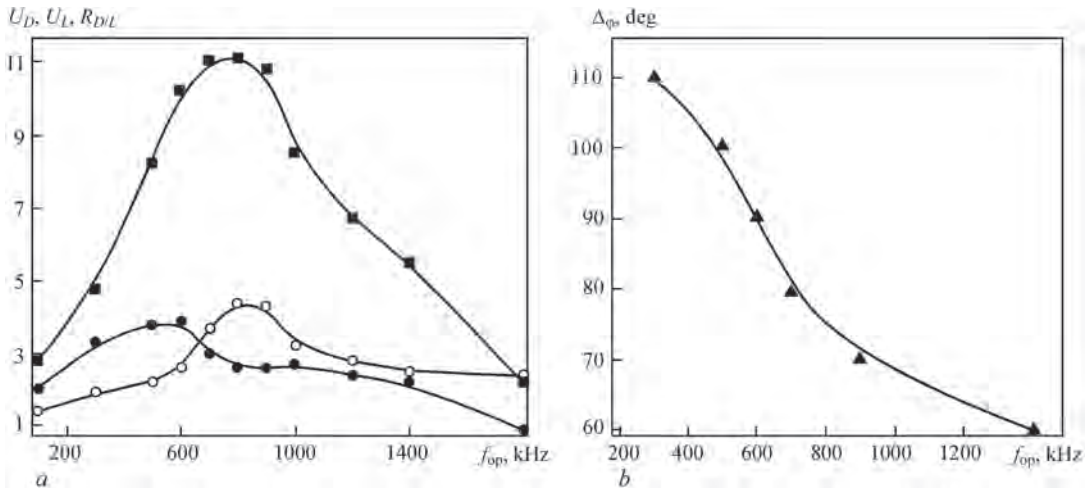


**Figure 4.** Dependences of the signal amplitude from a defect $U_D$ (■), change in clearance $U_L$ (●), and ratio $R_{D/L}$ (o) of the signal amplitude from a defect to the signal amplitude from the change in clearance on the operational frequency $f_{op}$ (*a*), as well as dependence of difference in Δφ (▲) of phase signal angles from a defect and change in clearance on the operational frequency $f_{op}$ (*b*)

tional frequency $f_{op}$, at which not only a sufficiently high level of signal amplitude from a defect $U_D$ can be achieved, but also the best ratio $R_{D/L}$ of the signal amplitude from a defect to the signal amplitude from the lift-off, which in our case is the amplitude of $U_L$ signal, caused by the change in clearance between the working surface of the ECP and TO surface during scanning. In addition, we have an additional opportunity to separate useful signals from defects and the change in the clearance by using a complex plane at different directions (different angles) of signals from a defect and signals from the change in clearance. The best conditions for distinguishing signals from defects against the background of signals from the lift-off are in general performed when we have a right angle (Δφ = 90°) between them. But from the practical experience, the lesser difference of directions (but higher than 60°) can also be effectively used, because in this case the angle can be increased by the choice of different sensitivity on the orthogonal ECFD channels. The factor of signals direction in the complex plane sometimes allows making compromise decisions and be crucial to choose the optimal operational frequency in difficult situations, when the amplitudes of signals from defects and lift-off are close.

Figure 4, *a* shows the dependences of the signal amplitude from a defect $U_D$, signal amplitude from the change in clearance $U_L$ and the ratio $R_{D/L}$ of the signal amplitude from a defect to the signal amplitude from the change in clearance on the operational frequency $f_{op}$ in the range of 100–1800 kHz. The signals from a defect were received by scanning the specimen in the zone of an artificial defect of 0.2 mm deep, which corresponds to the minimum crack size to be detected in blades in accordance with technical requirements. The amplitude of the signal caused by the change in clearance was evaluated by removing the ECP from the SS surface at a distance significantly larger than 10 mm. Amplitudes of signals from a defect and clearance are given in conditional values by divisions of the display scale of the eddy-current system, because the ratio of divisions and physical units of the signal amplitude is unknown due to lack of appropriate calibration.

Figure 4, *b* shows the dependence of the difference between the phase angles of signals from a defect and the change in clearance Δφ, which were evaluated according to the direction of hodograph signals in the complex ECFD plane with sufficient accuracy for practice.

It should be noted that the amplitude of signals from defects is high enough to detect them in the whole range of frequencies (100–1800 kHz). The largest amplitudes of signals from a defect of 0.2 mm deep are observed at the operational frequencies of 600–800 kHz (Figure 4, *a*), which can be considered as optimal by this criterion. But the best ratio of the signal from a defect to the signal from the lift-off is observed at the operational frequency of 800 kHz. Analysis of the change in the difference between the phase angles Δφ of signals (Figure 3, *b*) shows that according to this criterion, the operational frequency of 600 kHz is optimal, at which the angle between the useful signal from a defect and the signal from the change in clearance is close to the right one (90°). Taking into account the results analyzed above, the operational frequency of 700 kHz was determined as optimal. Subsequently, signals from defects were registered at this operational frequency.

To analyse the ECP sensitivity at different distance of the ECP from the TO surface, the registration of ECP signals from defects of 0.2 and 0.5 mm deep was performed at direct contact of the ECP with the TO

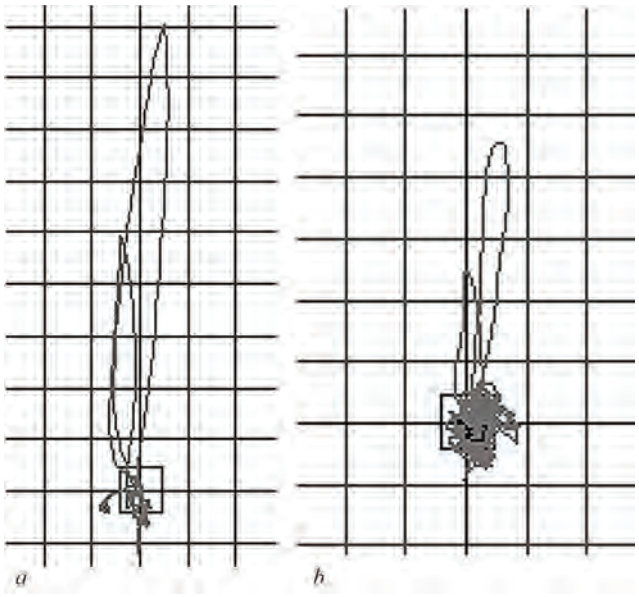

**Figure 5.** Signals caused by defects of 0.5 mm and 0.2 mm deep, at a direct contact of ECP with the specimen surface (*a*) and with the clearance of 0.5 mm in the complex plane (*b*)

surface and at a distance of 0.5 mm, provided by a dielectric plate of corresponding thickness.

Figure 5 shows signals caused by defects of 0.2 and 0.5 mm deep, in the complex ECFD plane at the operational frequency of 700 MHz, which were obtained at a zero distance of the ECP from the SS surface (*a*) and through a dielectric plate of 0.5 mm thick (*b*). In Figure 5, b signal registration sensitivity during scanning through a dielectric plate was increased by 12 dB to compensate for a significant decrease in amplitude.

Signals given in Figure 5 show the ability to detect a defect that characterizes the sensitivity threshold in depth (0.2 mm) with a sufficiently high signal/lift-off ratio even during inspection through a dielectric plate of 0.5 mm thick. We shoud note that for the ECP remoted from the TO surface at a distance of 0.5 mm (without a dielectric plate), the results will be similar. It is seen that the signal amplitude from a defect of 0.5 mm deep is approximately by 80 % higher than the amplitude of the signal induced by a defect of 0.2 mm deep, both for the case of direct contact of the ECP with the SS surface, as well as for inspection through

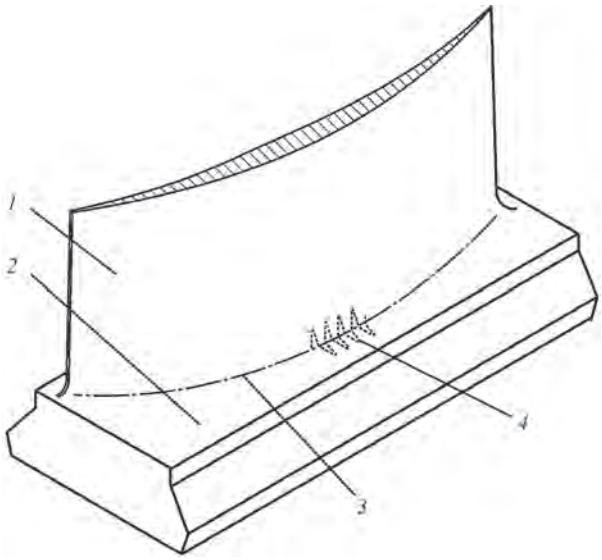

**Figure 7.** Zigzag trajectory of scanning fillet zone: *1* — blade airfoil; *2* — blade platform; *3* — fillet coupling line; *4* — scanning trajectory

a dielectric plate of 0.5 mm thick. Moreover, on the ECFD screen, electron noise can be observed, which at amplified sensitivity (Figure 5, *b*) is respectively more intensive by approximately 12 dB. In Figure 5, *a* signal from the change in clearance in the form of a small "shank" is observed, which is shifted to the left from the zero point, which corresponds to the compensation of the ECP imbalance during its installation on a defect-free area of the SS. In Figure 5, *b* signal from the change in clearance is already not observed, as far as the ECP was already remoted by 0.5 mm from the SS surface and sensitivity to the changes in clearance is significantly lower.

## TESTING OF THE PROPOSED IN-SERVICE EDDY-CURRENT FLAW-DETECTION TECHNIQUE FOR FILLET ZONES OF TURBINE BLADES

To inspect gas turbine blades without their disassembly (during inspection shutdown of turbine), a special ECP was produced, whose sensitive element by means of a thin pipe of austenitic steel of 3.5 mm diameter is remoted at a distance of 20 mm from the handle operated by the flaw detection operator. In this

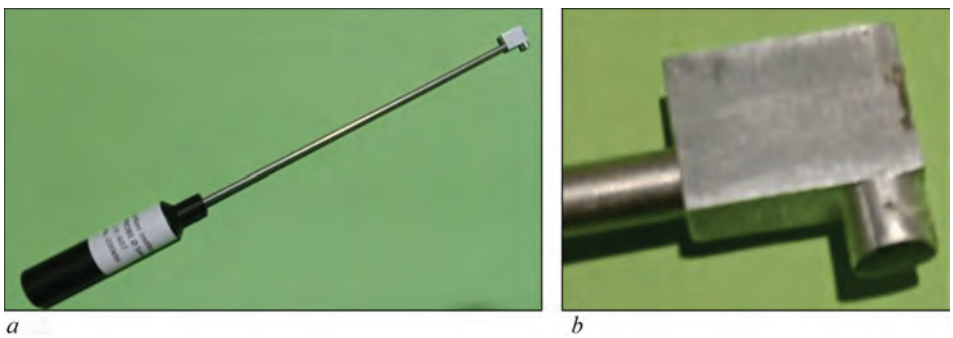

**Figure 6.** Eddy-current probe of MDF 0501 type with a remoted sensitive element: general appearance (*a*), sensitive ECP element (*b*)

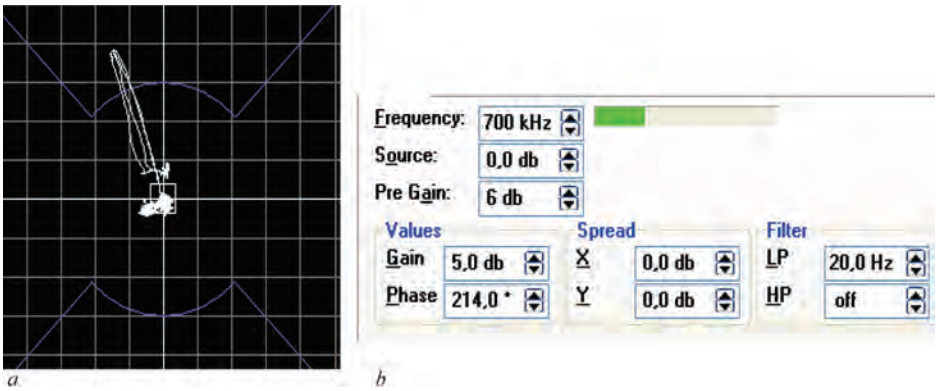


**Figure 8.** Signals from a short slot type defect (see Figure 1) in real blade (*a*) and displaying inspection parameters on the display (*b*)

**Figure 9.** In-service tests of the proposed eddy-current inspection technique of gas turbine blades

case, the sensitive element is oriented perpendicular to the handle axis (Figure 6).

Figure 7 schematically shows a blade fragment with a zigzag trajectory of manual scanning *4* of the fillet zone between the airfoil *1* and the platform *2* of a blade. In practice, this is performed by turning the ECP around the handle axis with its gradual advancement along the fillet. The step between the scanning lines is approximately 0.5 mm, that ensures a reliable detection of defects of more than 2 mm long. During scanning, the flaw detection operator should maintain the perpendicular position of the sensitive ECP element relative to the convex fillet surface. This operation requires some experience. Therefore, the flaw detection operator preliminary practices it on a real blade with an artificial defect (Figure 1).

The ECP of MDF 0501 type shown in Figure 6 with an elongated pipe was tested on a gas turbine compressor blade with an electro-erosion slot of 4 mm long, 0.2 mm deep and opening of 0.1 mm in the fillet zone, which is designed to adjust the equipment and check the inspection technique. The obtained results are shown in Figure 8, where the ECFD display in the mode of reproduction of a complex signal plane is depicted. The flaw detection pattern shows two signals from a defect close by amplitude, since the ECP crossed the defect zone twice. This made it possible to highly evaluate the repetition rate when receiving signals from defects. The signals from a defect are oriented and clearly fall into the sector frame of the automatic alarm. The signals caused by changes in clearance during zigzag scanning of the fillet zone at a distance from a defect, first, are significantly smaller relative to the signal from a defect, and secondly, are oriented to the left from the starting point (ECP balancing point), i.e. different in direction.

The tests showed that ECP of MDF 0501 type at selected optimal inspection parameters is characterized by high sensitivity and selectivity of inspection even under the conditions of manual scanning. The set sensitivity parameters of the ECFD use only a small part of capabilities for amplification of ECP signals (Figure 8, *b*).

The developed in-service eddy-current flaw detection technique for blades was successfully tested at gas turbines of the Nuovo Pignone SPA Company (Florence, Italy), which is a regional representative of an American multisectoral corporation General Electric (https://ge-nuovopignone.com) (Figure 9).

## CONCLUSIONS

The results of experimental studies aimed at creating effective eddy-current flaw detection technique of a critical fillet zone of gas turbine blades fabricated of ferromagnetic steels were considered. The proposed inspection technique was implemented by using selective double differentiation ECP, which provide high sensitivity during inspection in the conditions of changes in clearance between the working surface of the ECP and blade surface in the fillet zone. A comprehensive approach to the optimal choice of

the operational frequency was proposed. The carried out studies of signals of the ECP of MDF 0501 type (working surface diameter is 5 mm) allowed minimizing the lift-off effect by selecting the operational frequency and choosing the scanning parameters of the inspected zone, which is confirmed on a real blade with an artificial defect of 2 mm long and 0.2 mm deep, which characterizes the sensitivity threshold set by the technical assignment. The effectiveness of the proposed technique is confirmed during its tests at entrprises of the power engineering, in particular in gas turbines of the Nuovo Pignone SPA Company (Florence, Italy).

## REFERENCES


1. Benini, E. (2011) *Advances in gas turbine technology.* InTech, Rijeka, Croatia. www.intechopen.com
2. Mane, S. (2023) Advancements in gas turbine engine technology: A conceptual aspect. *Inter. J. of Enhanced Reseach in Science, Technology & Engineering*, 12(**7**), 37–41. DOI: https://doi.org/10.55948/IJERSTE.2023.0706
3. Subbotovich, V.P., Yudin, Yu.A., Yudin, A.Yu., Boyarshinov, A.Yu. (2013) Research of the turbine rotor blade hub zone. *NTU "KhPI: Bulletin: Power and Heat Eng. Proc. and Equipment*, 987(**13**), 34–37 [in Russian].
4. Sameezadeh, M., Farhangi, H. (2012) *Fracture analyzes of generator fan blades.* Applied Fracture Mechanics, Rijeka, InTech, 311–330. www.intechopen.com.
5. Rajabinezhad, M., Bahrami, A., Mousavinia, M. et al. (2020) Corrosion-fatigue failure of gas-turbine blades in an oil and gas production plant. *Materials*, 13(**4**), 900. DOI: https://doi.org/10.3390/ma13040900
6. Abassi, W., Rahman, S., Metala M. (2008) *NDE techniques and lifetime assessment of turbine equipment*. Power-Gen International, Orlando Florida.
7. Pitkänen, J., Hakkarainen, T., Jeskanen, H. et al. (2000) NDT methods for revealing anomalies and defects in gas turbine blades. In: *Proc. of 15th World Conf. on Non-Destructive Testing, Rome*. www.ndt.net.
8. Abassi, W., Fair, M. (2006) Ultrasonic phased array inspection of turbine components. In: *Proc. of 9th European Conf. on Non-Destructive Testing, Berlin.* www.ndt.net.
9. Libby, H. (1971) *Introduction to electromagnetic nondestructive test methods*. Wiley-Interscience, New York, NY, USA.
10. Udpa, S.S., More, P.O. (2004) *Nondestructive testing handbook (third edition).* Vol. 5, Electromagnetic Testing, American Society for NDT.
11. Garcíamartín, J., Gómezgil, J., Vázquezsánchez, E. (2011) Non-destructive techniques based on eddy current testing. *Sensors,* **11**, 2525–2565. DOI: https://doi.org/10.3390/s110302525
12. Helifa, B., Oulhadj, A., Benbelghit, A. et al. (2006) Detection and measurement of surface cracks in ferromagnetic materials using eddy current testing. *NDT&EInter.,* **39**, 384–390. DOI: https://doi.org/10.1016/j.ndteint.2005.11.004
13. Jansen, H. (2012) Eddy current testing: profiled eddy current probes for complex shape iInspection. In: *Proc. of 18th World Conf. on Non-Destructive Testing, Durban*. www.ndt.net
14. Nath, S.C., Batzinger, T.J., Rose, C.Met al. (2004) *Method for in-situ eddy current inspection of coated components in turbine engines*. US Pat. 6707297, G01N27/82, GE Company, Publ. 16.03.2004.
15. Tian, G.Y., Sophian, A. (2005) Reduction of lift-off effects for pulsed eddy current NDT. *NDT&EInter.,* **38**, 319–324. DOI: https://doi.org/10.1016/j.ndteint.2004.09.007
16. Kuts, Y., Lysenko, J., Dugin, A., Zakrevskii, A. (2016) Analysis of an eddy-current transducer with impulsive excitation in the nondestructive testing of cylindrical objects. *Materials Sci.*, 52(**3**), 431–437. DOI: https://doi.org/10.1007/s11003-016-9975-4
17. Uchanin, V., Nardoni, G. (2019) Detection of cracks in ferrous steel structures: new innovative eddy current techniques. *Procedia Structural Integrity*, **16**, 198–204. DOI: https://doi.org/10.1016/j.prostr.2019.07.041
18. Uchanin, V., Nardoni, G. (2013) Eddy current detection of cracks in ferromagnetic steel structures. In: *The Fundamentals of Structural Integrity and Failure*. Ed. By M. Richard. Wilcox, Nova Science Publishers, NY, USA, 193–221.
19. Uchanin, V.M., Ivashchenko, K.A. (2021) Detection of defects of structures from ferromagnetic steel through the layer of anticorrosion cover without removal. *Methods and Devices of Quality Control*, 1(**46**), 5–14 [in Ukrainian]. DOI: https://doi.org/10.31471/1993-9981-2021-1(46)-5-14
20. Uchanin, V. (2023) Surface eddy current probes of double differential type as an effective tool to solve non-destructive inspection problems. *The Paton Welding J.*, **2**, 46–55. DOI: https://doi.org/10.37434/tpwj2023.02.07


## ORCID

V. Uchanin: 0000-0001-9664-2101

## CONFLICT OF INTEREST

The Authors declare no conflict of interest

## CORRESPONDING AUTHOR

V. Uchanin
G.V. Karpenko Physico-Mechanical Institute of the NASU
5 Naukova Str., 79060, Lviv, Ukraine.
E-mail: vuchanin@gmail.com

## SUGGESTED CITATION

V. Uchanin, G. Nardoni, P. Nardoni (2024) Fatigue cracks detection in the fillet zone of steel blades of industrial gas turbines using eddy current method. *The Paton Welding J.*, **7**, 22–28.
DOI: https://doi.org/10.37434/tpwj2024.07.04

## JOURNAL HOME PAGE

https://patonpublishinghouse.com/eng/journals/tpwj

Received: 11.04.2024
Received in revised form: 12.06.2024
Accepted: 31.07.2024

DOI: https://doi.org/10.37434/tpwj2024.07.05

# PRACTICE OF IMPLEMENTING THE METHODOLOGY OF RISK ANALYSIS OF THE OPERATION OF WELDED METAL STRUCTURES IN UKRAINE

**V.M. Torop**

E.O. Paton Electric Welding Institute of the NASU
11 Kazymyr Malevych Str., 03150, Kyiv, Ukraine

**ABSTRACT**

The development of standard approaches, regulatory response measures and coordinated actions at the international, regional, national and local levels is the best and perhaps the only means of influencing the risk, which can have negative consequences in the form of failure, accidents, and catastrophes. This task requires an urgent solution, because the number of risks in the modern world is increasing. One of the main goals established by the ISO 31000 standard is the continuous improvement of risk management in organizations based on a general model intended for adaptation to a wide range of risks. This publication is devoted to a historical overview of the state of affairs regarding the implementation of the risk analysis methodology in Ukraine and the practice of its use for welded metal structures.

**KEYWORDS:** risk, standardization, integrity management, E.O. Paton bridge

## INTRODUCTION

Full-scale war with the Russian Federation, drone attacks on energy and infrastructure objects, missile, artillery and mortar shelling of border areas and territories in the area of hostilities, terrorism, cyberattacks, raiding, reputational damage, etc. is only a small list of threats that fill our lives daily. Each of these threats has a risk to be realized. And realization of a threat affects the related losses. The scale of losses depends on the subject for which this threat exists. It can be the world, a country, an organization, a person.

There risk always exists, but obviously making management decisions on risk reduction requires a structured approach. In the fundamental article [1], the urgency of implementing the risk assessment system in Ukraine is attributed by the author to the problem of national security. Let's bring a very eloquent quote from it: "A gap of our state in this field becomes threatening. This results not only in discrediting of the Ukrainian science, but also in the inefficiency of the national industry, its high accident rate and, which is more frightening, in unreasonable human victims. Due to the fact that the task of risk assessment can be considered as a task of making a multicriteria collective decision, which requires studying of a wide range of issues in the technical, economic and social areas of life, there is a need to create a system of administrative risk management in Ukraine.

This state of affairs is partially predetermined by the lack of a state approach to the risk management in the former Soviet Union, where the price of human safety and ecology was by no means high. As the authors noted [2]: "... in the ten-volume edition "Reliability and efficiency in engineering", published during 1987–1990, the concept of risk analysis is not even mentioned. Similarly, many of its important components are not described, for example, the techniques for calculating the consequences of accidents manifested in their impact on human health or economic indicators, the techniques for assessment of the probability of failure on the basis of physical models both with the help of approximate analytical approaches as well as numerical modeling by the Monte Carlo method or its derivatives. At the same time, the responsibility for the absence of both standards on risk as well as reliability (one of the risk components) of industrial objects in Ukraine is equally held both on scientists in the field of strength and reliability, as well as on officials who should provide supervision of labor safety".

The concept of risk is extremely broad and in the article cited above [1] and fundamental works [3–5], some of its aspects, definitions and use in various fields of science, engineering and human activity are given. The task of technical specialists consists in disclosing its content and implementation in certain industries. It is important here to take into account international experience, real technical capabilities of industry and modern achievements of scientists.

## IMPLEMENTATION OF RISK ANALYSIS METHODOLOGY IN UKRAINE

The practice of implementing the risk analysis methodology in Ukraine originates with the adoption of the Law of Ukraine "On objects of increased danger" (Vidomosti Verkhovnoyi Rady Ukrainy, 2001,

No. 15, Article 73 with the following amendments) [6]. According to the procedure for declaring the safety of objects of increased danger, which is determined by the Decree of the Cabinet of Ministers of Ukraine dated July 11 2002 No. 956 [7], the level of risk is assessed in accordance with the Methodology for determination of risks and their acceptable levels for declaring the safety of objects of increased danger, which is approved by the Order of the Ministry of Labor and Social Policy No. 637 dated December 04 2002.

The government of Ukraine in the framework of the Kyoto Program of 2005–2015 in January 2014 approved the "Concept of risk management of man-made and natural emergencies", approved by the Decree of the Cabinet of Ministers of Ukraine No. 37-p dated January 22 2014 [8].

The main purpose of the Concept is to achieve the acceptable levels of risks throughout the Ukraine, which is implemented in the next stages:

1) to determine the risk levels for all sectors of the economy and the most dangerous sources of emergencies and ensure their reduction to accepted risk levels;

2) to reach the risk level throughout the Ukraine in accordance with terms used in economically developed countries.

The Concept implementation plan for 2015–2020 provided the creation of the following guides:

- organizational guide: workshops, scientific conferences on the implementation of danger management system in Ukraine during emergency situations of man-made and natural character;
- guide of normative legal acts: improvement of legislative norms on implementation of approaches based on risks;
- methodical guide: development of risk assessment methodology by research institutions, systematization according to the types of emergency situations;
- educational guide: curricula for experts on risk management in the field of man-made and natural safety.

In order to implement the Sendai Framework for Disaster Risk Reduction for 2015–2030 [9], adopted by the III UN World Conference in Sendai, Japan on March 18 2015, the Cabinet of Ministers of Ukraine approved the Strategy for Reforming the State Emergency Service of Ukraine, which, among other things, envisages a full-scale reformation of the state system for response to emergencies and improvement of its ability to struggle natural and man-made threats. The Sendai Framework for Disaster Risk Reduction for 2015–2030 outlined seven clear goals and four priorities for preventing new and reducing existing risks of natural hazards:

- understanding the risk of natural hazards;
- strengthening in management of risks of natural hazards;
- investments in reducing the risks of natural hazards;
- increase in readiness to natural hazards for effective response and obtaining the best practices during restoration, rehabilitation and reconstruction.

The Sendai Framework is aimed at achieving a significant reduction in the risk of disasters and losses of life, livelihoods and health, as well as economic, physical, social, cultural and environmental assets of people, enterprises, communities and countries over the next 15 years.

In addition, in the framework of the Association Agreement between Ukraine, on the one hand, and the European Union, the European Atomic Energy Community and their member states, on the other hand, a plan for implementation of some EU legislative acts was developed (approved by the Cabinet of Ministers of Ukraine on October 25 2017, No. 1106), [10] that envisages the execution of:

- Directive 2012/18/EU of the European Parliament and of the Council of 4 July 2012 "On the control of major-accident hazards involving dangerous substances";
- Directive 2007/60/EU of the European Parliament and of the Council of October 23 2007 "On the assessment and management of flood risks".

In order to reduce losses and trying to standardize the algorithm of actions in case of manifestation of one or another risk, summarizing the world experience, in 2009 ISO — the International Organization for Standardization (https://www.iso.org) adopted a series of international standards for risk management, in particular:

- ISO Guide 73:2009 Risk management — Vocabulary (https://www.iso.org/standard/44651. html);
- ISO/IEC 31000:2009 Risk management — Principles and guidelines (https://www.iso.org/ standard/43170.html);
- ISO/IEC 31010:2009 Risk management — Risk assessment techniques (https://www.iso.org/ standard/51073.html).

In 2013, the guidance for the implementation of ISO 31000 ISO/TR 31004:2013 Risk management — Guidance for the implementation of ISO 31000 (https://www.iso.org/standard/56610.html) was published.

The above standards are the standards of the "upper-level" risk management. They were adopted as national standards by more than 50 national standard-

ization bodies covering more than 70 % of the world's population. They were also adopted by some UN organizations and national governmental organizations as a basis for the development of the own risk-oriented standards and techniques.

According to the plan of implementation of the international legislative framework, in accordance with the Law of Ukraine "On Standardization" dated June 05 2014, No. 1315-VII [11], analogues of international standards of 2009 were adopted in Ukraine:

- DSTU ISO Guide 73:2013 "Risk management. Vocabulary" [12];
- DSTU ISO 31000:2014 "Risk management. Principles and Guidelines" [13];
- DSTU ISO/IEC 31010:2013 "Risk management. General risk assessment techniques" [14].

## DEVELOPMENT OF RISK ANALYSIS IN THE WORLD

The development of international standards, regulatory response measures and coordinated actions at international, regional, national and local levels is the best and perhaps the only means of influencing the risk that has potentially global consequences. This task requires an urgent solution, as far as a number of risks on a global scale is growing. One of the main goals established by ISO 31000 [13] is the constant improvement of the risk management in the organizations on the base of a general model intended for adaptation to a wide range of risks.

Although according to the ISO regulations, any standard should be revised every five years, the ISO 31000 Basic Risk Management Standard has been valid for almost nine years. During this time, a considerable experience in the field of risk management was accumulated. Yesterday's risk management practices are not adequate to struggle today's threats. These mechanisms need to be upgraded. Such derivatives became a cause for revision of the ISO 31000 standard [13].

A new guide was published in 2018 to help users to fully optimize its meaning. ISO 31000:2018 "Risks management" is a practical guide that helps organizations to integrate an effective decision-making structure into their management, leadership and culture by the optimal use of ISO 31000.

The standard itself explains the fundamental concepts and principles of risk management, simultaneously describing the structure and outlining the processes for risk identification and management. It provides extended information and context to the sections of ISO 31000, including guidelines for developing a plan for risk integration into the existing organization's document management, communications with concerned parties, monitoring and revision of the risk management plan and many other.

ISO 31000:2018 [13] was elaborated in cooperation with UNIDO (the UN Industrial Development Organization). ISO 31000:2018 is a brief guide to help organizations in appplying risk management principles to improve planning and making more effective solutions.

At the official site of ISO [https://www.iso.org/home.html], the main changes to the previous version of the standard are presented, such as:

1. Analysis of the risk management principles is carried out that are hyper-significant success criteria.

2. Attention is focused on the leadership of senior management, which should ensure the integration of risk management, extend it to all processes, starting with the organization management.

Hence, ISO 31000 is the standard of risk management, which was adopted in 90 % of the greatest world economies.

In June 2019, on the website of the International Organization on Standardization (ISO), the second issue of the International Standard IEC 31010:2019 (Risk management — Risk assessment techniques) is available [14]. According to the ISO website "... this document provides guidelines on the choice and application of risk assessment techniques in a wide range of situations. The techniques are used to assist in making decisions with uncertainty, to provide information on certain risks and as a part of the risk management process. This second issue cancels and replaces the first issue, published in 2009. In the document, the process of planning, implementation, verification and confirmation of the use of techniques is considered in more details; a number and scope of techniques was increased.

IEC 31010 was prepared by the 56th Technical Committee "Reliability" of the International Electrotechnical Commission (IEC) together with 262 T3 ISO. This standard complements the ISO 31000 provisions [13].

ISO/IEC 31010 focuses on concepts, processes and the choice of a risk assessment technique, provides a basis for making decisions on applying the most appropriate approach to specific risk assessment. The standard provides examples of different risk assessment techniques (including brainstorming, Delphi method, "preliminary hazard analysis", HAZOP, HACCP, FMEA, FTA, Decision Tree, Swift Technology, Monte Carlo Method, etc. — 31 techniques in total) and references to other international standards are given, describing their application in more detail.

## INFORMATION AND ANALYTICAL SYSTEM FOR MANAGEMENT OF TECHNICAL CONDITION AND INTEGRITY OF PIPELINE TRANSPORT NETWORK OBJECTS "ITT-PIMS"

Ukraine has to build a new management system on the basis of an approach based on a risk assessment that is a part of the management process and also has a fundamental importance for organisation management at all levels.

For example, the Operator of the gas transportation system of Ukraine (OGTSU) since 2021 introduces the Information and Analytical System for Management of Technical Condition and Integrity of Pipeline Transport Network Objects "ITT-PIMS". This software complex offers information system to manage processes for gas transportation systems PIMS (Pipeline Integrity Management Systems). The software product will allow implementing a comprehensive assessment of the technical condition and safety of functioning of main gas pipelines, determining the technical condition of infrastructure, assessing risks, developing plans for their prevention and reduction of the consequences of possible accidents.

The information-analytical system consists of 52 modules and three subsystems aimed at the following processes and tasks:

- formation of a spatial database of objects of a linear part of main gas pipelines (LPMG) and their objects in the environment, development of tools for management of spatial data;
- certification of basic and auxiliary equipment and systems, development of tool for management of technological information;
- graphical display of data on LPMG and objects in the environment;
- management of spatial and monitoring data of air patrol (including photos /video fixation of violations of security zones of a main gas pipeline (MG);
- technological document management of units from the direction of LPMG operation, documentation management, reporting;
- land registry of the territories of MG passage;
- management of results of diagnostics and repairs of LPMG objects, interpretation of results;
- analytical assessment of the technical condition of LPMG objects (including integrated assessment by a defined group of criteria);
- LPMG operation risk management;
- repair planning;
- LPMG repair budget management;
- integration of the system with the "Complex automated management system" (CAMS) based on SAP ERP etc.

It should be noted that in the practical application of the risk analysis methodology, a number of problems arises related to the uncertainty of choosing mathematical methods, physical models and input data. This is especially true for the uncertainty in the real distribution of probabilistic values characterizing the object condition or external factors, amplitudes and the frequency of certain natural disasters. This casts doubt on the confidence in absolute initial numerical values. Without a detailed description and discussion of all uncertainties and ambiguities accepted in the analysis, the practical application of such absolute values should be quite limited. For example, comparison of the results with the admissible risk criteria declared in norms or standards (which finds ever more widespread use in the world) becomes simply mathematical exercises. Therefore, the specification of input data, creation of an appropriate correct calculation model, the use of modern technologies, algorithms, systematic approach and standardization of principles for implementation of risk analysis for each specific industry or human activity becomes an urgent need. One of the examples of the practical implementation of the above approaches is the "Methodology for determination of the risk of operating physically worn or morally obsolete welded metal structures that do not meet the requirements of labor protection and pose a potential threat to the life and health of workers" developed at the PWI of NASU [15].

## USE OF RISK ANALYSIS IN THE INSPECTION OF THE TECHNICAL CONDITION OF THE E.O. PATON BRIDGE

The results of inspecting the corrosion damage to the main beams of the E.O. Paton bridge across the Dnipro River in Kyiv indicates that as a result of draining rainwater and water formed as a result of snow melting (contains salts) through deformation welds on welded metal structures of the main beams, whose metal of the end sections of the spans is adjacent to the deformation welds, was exposed to local and, in some places, significant corrosion damages. Due to corrosion, the thickness of the metal in the structural elements, namely in the lower girths, lower horizontal stiffeners and in the lower part of the walls of the main beams decreased significantly. In some cases (for example, in the spans F10 and F15 of the main beam No. 1 and the spans F1 and F3 of the main beam No. 4), the thickness of the walls decreased by 40–50 % [16, 17]. The presence of such corrosion damages can significantly reduce the fatigue failure resistance of welded joints with detected defects, which indicates an increase in the risk of failure of

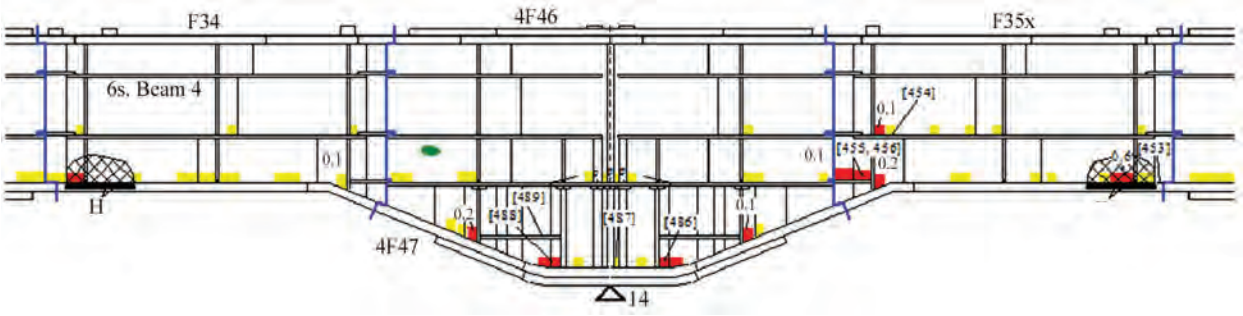


**Figure 1.** Results of measuring thickness of the span wall and voute for the span F46 of the main beam No. 4 [17]

**Figure 2.** Crack formed in the zone of corrosion thinning of the weld in the span F46 of the main beam No. 4

the span structure in case of further propagation of corrosion processes.

For example, Figure 1 presents the results of 133 measurements of the span wall thickness and 113 measurements of the thickness of the voutes for the span F46 of the main beam No. 4 [16, 17]. Corrosion damages of 2–4 mm depth were detected (marked with a yellow marker) and of more than 4 mm (red). Nonmetallic inclusions are marked with a green marker.

The smaller the number of measurements, the greater the risk of missing a defect. In addition, corrosion thinning in the weld zone can serve as an additional source of corrosion cracks, which is illustrated by Figure 2.

According to our developed "Methodology for determining the risk of operation of welded metal structures..." [15], the risk of operation of the span F46 of the main beam No. 4 is determined by the 4C index at the risk matrix, which is shown in Figure 3 and corresponds to the pre-accident condition of the main beams of the E.O. Paton bridge, the probability of failure reaches a value of 0.8.

According to the recommendations [15], the orange area of the risk matrix provides for the need to develop and approve the "Security Declaration" with the regulator (Department of Supervision in Industry and at Objects of Increased Danger of the State Labor of Ukraine) including a report, a plan of measures to eliminate drawbacks and carry out improvement measures for the operation of the main beams of the

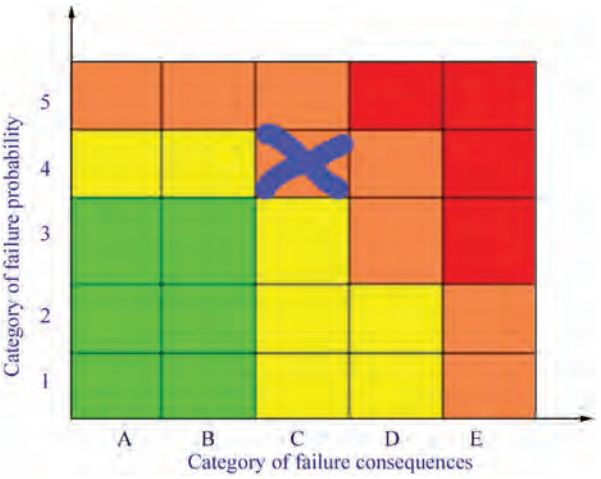


**Figure 3.** Risk matrix for the operation of the span F46 of the main beam No. 4 of the E.O. Paton bridge

E.O. Paton bridge. In addition, it is necessary to develop a plan, to justify the choice of techniques, to determine and to agree the term of diagnostics and technical inspection, which also provides a mandatory detailed analysis of the risk for the further operation of the main beams of the E.O. Paton bridge.

## CONCLUSIONS

1. Ukraine should build a system for management of the integrity of welded metal structures for objects of increased danger based on the approach using modern technologies and algorithms of system analysis, standardization of principles to implement risk analysis for each specific industry.

2. Risk assessment is a part of the management process, and has a fundamental importance for the enterprise management at all levels of its activity. Therefore, the introduction of the Methodology [15] can serve as an example of the practical implementation of the best modern world practices in providing reliable and safe operation of welded metal structures for objects of increased danger.

3. Implementation of risk analysis will provide new partner relations between the operator, operating potentially dangerous objects and the regulator — supervisory body of the state.

## REFERENCES


1. Kachynsky, A.B. (2002) Development of the risk problem in Ukraine: Theory and practice. *Strategic Panorama*, **4**, 14–25 [in Ukrainian]
2. Torop, V.M., Torop, O.V. (2004) Implementation of risk analysis in the system of ensuring the integrity of main pipelines. In: *14th Inter. Business Meeting on Diagnostics 2004*, Moscow, 81–85 [in Russian].
3. Horbulin, V.P., Kachynskyi, A.B. (2010) *Strategic planning: Solving national security problems*. Kyiv, NISD [in Ukrainian]
4. Ivanyuta, S.P., Kachynskyi, A.B. (2012) *Ecological and natural and man-made security of Ukraine: Regional dimension of threats and risks*. Kyiv, NISD [in Ukrainian]
5. Makhutov, N.A., Gadenyn, M.M., Yudina, O.N. (2019) Scientific analysis of risks in life support of a person, society and state. *Problems of Risk Analysis*, 16(**2**), 70–86 [in Russian] DOI: https://doi.org/10.32686/1812-5220-2019-16-2-70-86
6. Law of Ukraine "On objects of increased danger" https://zakon.rada.gov.ua/laws/show/2245-14#Text [in Ukrainian].
7. Decree of the Cabinet of Ministers of Ukraine of July 11, 2002 No. *956 "On identification and declaration of safety of objects of increased danger"* [in Ukrainian]. https://zakon.rada
8. *The concept of man-made and natural emergency risk management*. Approved by the order of the Cabinet of Ministers of Ukraine No. 37 dated January 22, 2014 [in Ukrainian]. https://zakon.rada.gov.ua/laws/show/37-2014-%D1%80#Text
9. The Sendai Framework for Disaster Risk Reduction 2015-2030, Sendai, Japan, March 2015. https://www.undrr.org/publication/sendai-framework-disaster-risk-reduction-2015-2030
10. Resolution of the Cabinet of Ministers of Ukraine dated October 25, 2017 No. 1106 "*On the implementation of the Association Agreement between Ukraine, on the one hand, and the European Union, the European Atomic Energy Community and their member states, on the other hand"* [in Ukrainian]. https://zakon.rada.gov.ua/laws/show/1106-2017-%D0%BF#n36
11. Law of Ukraine on standardization (Vedomosti Verkhovna Rada (VVR), 2014, No. 31 [in Ukrainian]. https://zakononline.com.ua/documents/show/357896_693333
12. DSTU ISO Guide 73:2013: *Risk management. Dictionary of terms* [in Ukrainian]. https://khoda.gov.ua/image/catalog/files/dstu%2073.pdf
13. DSTU ISO 31000:2014: *Risk management. Principles and guidelines*. New version from 2018. DSTU ISO 31000:2018 *Risk management. Principles and guidelines* (ISO 31000:2018, IDT) [in Ukrainian]. https://online.budstandart.com/ua/catalog/doc-page.html?id_doc=80322
14. DSTU ISO/IEC 31010:2013: *Risk management. General risk assessment methods.* https://online.budstandart.com/ua/catalog/doc-page.html?id_doc=66723 or DSTU EN IEC 31010:2022 *Risk management – risk assessment methods* (EN IEC 31010:2019, IDT; IEC 31010:2019, IDT)
15. (2024) *Methodology for determining the risk of operating physically worn or morally obsolete welded metal structures that do not meet the requirements of labor protection and pose a potential threat to the life and health of workers.* Kyiv, PWI [in Ukrainian].
16. Poznyakov, V.D., Dyadin, V.P., Davydov, Ye.O., Dmytrienko R.I. (2021) Evaluation of damage of all-welded longitudinal main beams of the E.O. Paton bridge across the Dnipro river. *The Paton Welding J.*, **7**, 30–38 [in Ukrainian]. DOI: https://doi.org/10.37434/tpwg2021.07.06
17. Lobanov, L.M., Dyadin, V.P., Davydov, E.O., Lytvynenko, V.A. (2021) Selection of nondestructive testing methods for evaluation of the technical condition of metal structures of the main beams of E.O. Paton bridge across the Dnipro in Kyiv. *Tekh. Diahnost. ta Neruiniv. Kontrol*, **4**, 47–53 [in Ukrainian]. DOI: https://doi.org/10.37434/tdnk2021.04.05



## ORCID

V.M. Torop: 0000-0002-8807-9811

## CORRESPONDING AUTHOR

V.M. Torop
E.O. Paton Electric Welding Institute of the NASU
11 Kazymyr Malevych Str., 03150, Kyiv, Ukraine.
E-mail: v.torop@gmail.com



## SUGGESTED CITATION

V.M. Torop (2024) Practice of implementing the methodology of risk analysis of the operation of welded metal structures in Ukraine. *The Paton Welding J.*, **7**, 29–34.
DOI: https://doi.org/10.37434/tpwj2024.07.05

## JOURNAL HOME PAGE

https://patonpublishinghouse.com/eng/journals/tpwj

Received: 02.05.2024
Received in revised form: 11.06.2024
Accepted: 29.07.2024

DOI: https://doi.org/10.37434/tpwj2024.07.06

# OPTIMIZATION OF THE REFRACTORY LINING FOR FERROMANGANESE PRODUCTION FURNACE

**M.M. Gasik**

Aalto University, 00076 AALTO, Espoo, Finland

**ABSTRACT**

The methods of decreasing the lining corrosion rate by controlling the temperature mode are analyzed. It is shown that selection of a proper combination of refractory material layers would allow a noticeable decreasing the lining corrosion rate at interaction with liquid metal, but this also would increase heat losses due to convective and radiation heat transfer. A proper algorithm is suggested to reach the optimal solution by optimization of the lining layer thickness and composition.

**KEYWORDS:** furnace, lining, thermal mode, temperature distribution, ferromanganese, corrosion

## INTRODUCTION

Medium- and low-carbon ferromangaese is produced by the silicothermal process in ore reduction electric furnaces by reducing manganese from low-phosphorus slags by ferrosilicomanganese applying a three-stage scheme: manganese concentrate dephosphoration; smelting of processed silicomanganese; smelting of ferromanganese or metallic manganese [1–3]. According to the Ukrainian standard (DSTU 3547–97), ferromanganese, depending on the grade, has the following composition: 85–95 % Mn, <0.2 or <2.0 % C, <1.8 or < 3.0 % Si, <0.07 or <0.40 % P. Electric furnaces for smelting of such ferromanganese (Figure 1) have a magnesite lining, which is expected to provide a sufficiently long-term resistance to corrosion from molten Mn–Si–Fe ferroalloy and MnO–$SiO_2$–CaO slag [1–4]. The corrosion and destruction of a magnesite lining may be very significant if the slag has an elevated content of alkali metals ($NA_2O + K_2O$). These additives are used in the process in order to decrease the slag viscosity, especially at low temperatures, but their negative effect on the lining resistance can be much greater than the expected advantage due to control of the slag viscosity [5].

An improvement in the lining resistance can be solved by changing its composition (replacement of refractory materials by other), which changes the total thermal resistance of the heat insulating layer depending on the combination of thermal conductivity and layer geometry.

In [6], the temperature along the central axis of the furnace was calculated and the potential ability for reducing the lining corrosion rate was shown. The temperature distribution was estimated for a dense magnesite lining and when replacing a part of the lower layer with a magnesium-carbon brick having higher thermal conductivity. The idea consisted in reducing the temperature of the upper layer to its level close to the liquidus temperature of the ferro-alloy of the known composition and accordingly to delayering of the kinetics of the reaction of metal components with magnesite. The end results mentioned in [6] prove the potential ability for almost 5 times increase in the lining resistance, but due to greater heat losses. A significant disadvantage of these calculations is the inconsistency of parameters. They did not present any specific data on the heat flux, and the values of parameters differ between the text and figures. Our attempts to reproduce these results by using the same lining composition and geometry for such limiting conditions were not successful. In order to check these calculations and develop a justified concept of furnace lining, in this research the disadvantages of the method [6] were analyzed and the algorithm for evaluating the thermal parameters of lining of the furnace for smelting a middle and low-carbon ferromanganese.

## FURNACE MODEL AND COMPLIANCE WITH PARAMETERS

The first model of electric furnace for smelting of a medium-carbon ferromanganese was taken from [6] with parameters (Table 1), to which the main values of properties of refractory materials were added [3, 7, 8]. Other parameters were the same as in [6], except for those (the same materials or temperature) that differed beteen each other. Some of the mentioned values were optimized in [6] but without explanation of the exact way how it was done, which does not allow checking the calculations properly.

An additional analysis was conducted to justify the main variable parameters of the furnace thermal mode. The casing-air heat transfer coefficient $\alpha_c$ was taken into account as the function of the casing tem-

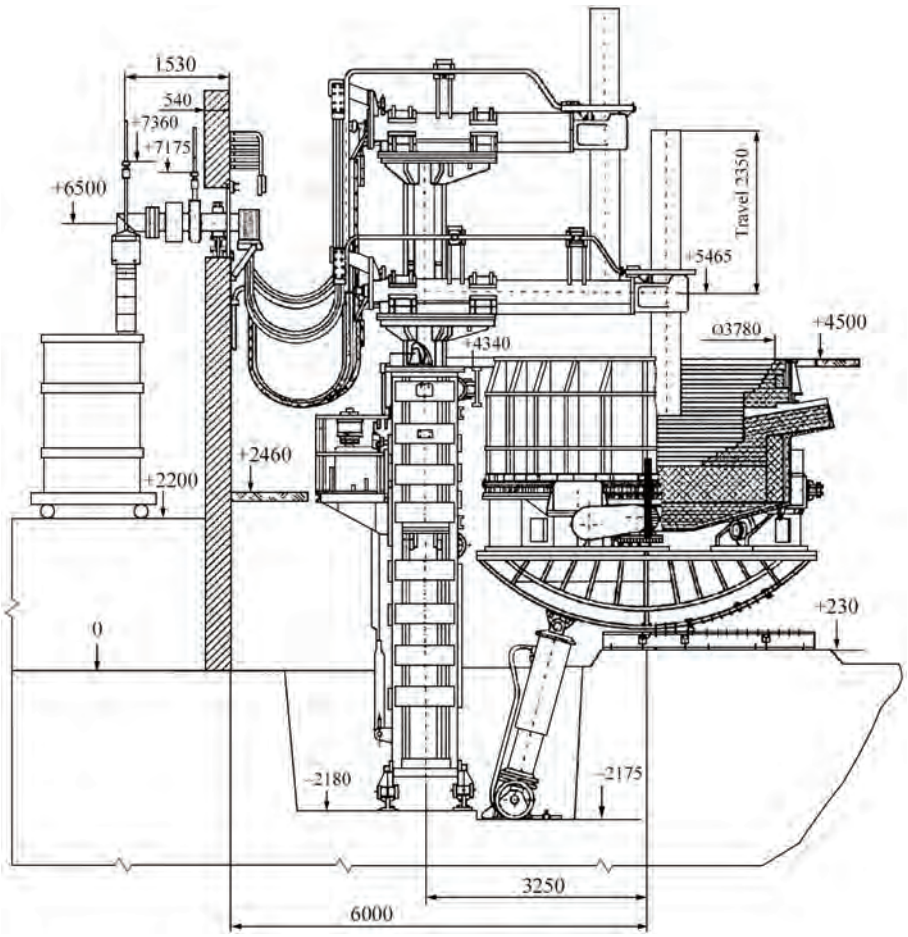


**Figure 1.** Typical furnace for smelting ferromanganese by silicothermal process [1, 3, 4]

perature $\alpha_c = 7.7743 + 0.0061t_c$ including natural convection and radiation heat exchange [8]. The overall Fourier metal-environment (air) heat transfer equation has the following appearance:

$$q = \frac{t_m - t_0}{\frac{1}{\alpha_m} + R_{th} + \frac{1}{\alpha_c}}; \quad R_{th} = \sum \frac{H_i}{\lambda_i}, \qquad (1)$$

where $q$ is the total heat flux through the lining along the central axis; $t_m$ and $t_0$ are the temperatures of metal and surrounding air (~ 30 °C), respectively; $\alpha_m$ and $\alpha_c$ are the metal-lining and casing-air heat transfer coefficients, respectively; $R_{th}$ is the total thermal resistance of the lining; $H_i$ is the height of each lining layer; $\lambda_i$ is the thermal conductivity of the layer material. To check the results [6], the total heat flux (1) can be evaluated according to data of Table 1: $q = (t_m - t_{cm})\cdot\alpha_m = (1350–1262)\cdot 18 = 1584$ W/m$^2$, which is a constant at a stationary furnace operation. However, according to [6], for the magnesite height $H = 0.585$ m at its thermal conductivity $\lambda = 10$ W/m·K, the heat flux (1)

**Table 1.** Parameters of furnace and lining

| Index | Work [6]* | Data of [3, 7, 8] and this work |
|---|---|---|
| Thermal conductivity of materials, W/m·K: | | |
| ● magnesite-carbon brick | 25 | 25 |
| ● sintered magnesite | 5 (Figure 4), 10, 11 (Text) | 10 |
| ● sintered dolomite | – | 5.8 |
| ● fireclay brick | – | 1.2 |
| Temperature across the central axis of furnace, °C: | | |
| ● outer casing ($t_c$) | 196 (Figure 3), 150 (Text) | Variable |
| ● casing in contact with metal ($t_{cm}$) | 1262 (Figure 3) | –»– |
| ● metal melt ($t_m$) | 1350 | 1350 |
| ● metal liquidus (80 % Mn, 0.80 % Si) | 1180 | 1180 |
| Other parameters, W/m$^2$·K: | | |
| ● metal–casing heat transfer ($\alpha_m$) | 18 | Depends on the Nusselt number |
| ● casing-air heat transfer ($\alpha_c$) | – | Depends on the temperature |
| *In [6], for the same parameters different data in the figures and in the text are shown. | | |

should be equal to $q = (t_{cm} - t_c)/(H/\lambda) = (1262–196)/(0.585/10) = 18220$ W/m$^2$, i.e. almost 10 times higher than the value based on $\alpha_m = 18$ W/m$^2$·K. If the value $q = 18220$ W/m$^2$ is considered correct, then the metal-lining heat transfer coefficient $\alpha_m$ should be equal to ~207 and not 18 W/m$^2$·K. At such a high heat flux and the casing temperature $t_c = 196$ °C, the heat transfer coefficient $\alpha_c$ should be ~103 W/m$^2$·K, which is impossible in the case of natural convection and radiation [8]. For a lower heat flux of 1584 W/m$^2$, the thermal resistance of magnesite should be (1262–196)/1584 = 0.673 m$^2$·K /W, which at the magnesite layer height $H = 0.585$ m [6] corresponds to its effective thermal conductivity $\lambda = 0.585/0.673 = 0.87$ W/m·K. This is much lower than the values 5 and 10–11 W/m·K given in [6] and lower than the data 4–5 W/m·K in the reference book [8]. Accepting the thermal conductivity of magnesite being $\lambda \sim 5$ W/m·K, this leads to the non-physical values of the heat exchange coefficients and the much higher casing temperature for the same lining geometry. Thus, data of [6] are inconsistent and prevent the correct evaluation of the furnace lining thermal mode.

## CALCULATION OF TEMPERATURE MODE

To obtain the correct values of the furnace thermal mode, in this work at first the parameters were taken, the values of which are undoubted: metal temperature, lining geometry and thermal conductivity of refractory materials (Table 1). The thermal flux should be self-consistent with the known heat transfer coefficients, so at the above heat flux of ~1584 W/m$^2$, the furnace-environment heat transfer coefficient $\alpha_c$ will amount to ~9.54 W/m$^2$·K, which is closer to 8.97 W/m$^2$·K (at $t_c = 196$ °C) for natural convection with a radiation component according to [8]. In this case, the metal-lining heat transfer coefficient $\alpha_m$ is really closer to 18 than to 207 W/m$^2$·K. However, at $\alpha_c \sim 10$ W/m$^2$·K and $\alpha_m \sim 18$ W/m$^2$·K, it is impossible to obtain the same temperatures as given in [6] if a part of a magnesite lining ($\lambda = 5$ W/m·K) is replaced by magnesium and carbon ($\lambda = 25$ W/m·K). This leads to either non-physical values of heat flux and heat transfer coefficients, or temperatures.

Thus, the correct method for calculation of lining properties and structure should be based on the self-consistent initial conditions (metal and casing temperature, thermal conductivity of refractory materials, correct heat transfer coefficients). Heat transfer coefficients can be changed if the free surface of the casing is exposed to forced convection with compressed air or water.

## EVALUATION OF CORROSION RESISTANCE OF LINING

It is known that resistance of a dense lining in contact with the molten metal can be estimated through its chemical degradation, since the contribution of the infiltration component is much smaller. For a porous lining, the situation can be inverse, where infiltration with the liquid metal reaches lower horizons [3, 6, 9]. Using a method similar to that taken in [6], the rate of chemical degradation of the lining ($v$, cm/h) during its contact with a middle-carbon ferromanganese can be estimated as follows:

$$v = 0.332\,\mathrm{Re}^{1/2}\,\mathrm{Sc}^{1/3}\left(\frac{D_i}{L}\right)\frac{\rho_{Me}}{\rho_{MgO}}\left(\frac{100}{\%\,x}\right), \qquad (2)$$

where Re is the Reynolds number [6, 8] for the motion (convection) of metal near the bottom-plate; Sc is the Schmidt number [6, 8]; $D_i$ is the diffusion coefficient of active mental components (in this case mostly for silicon); $L$ is the characteristic length of the furnace; $\rho_{Me}$ is the density of metal at a temperature $t_m$; $\rho_{MgO}$ is the lining density (magnesite); % $x$ is the magnesite fraction that can be dissolved by metal (taken in 5 %). Choosing the value of the parameters, it can be evaluated that the expected corrosion rate of magnesite (2) at $t_{xm} = 1262$ °C (the temperature at the lower point of the bottom-plate in contact with metal) will amount to ~0.275 cm/h at 0.80 % Si in the ferromanganese. A significant decrease in corrosion can be achieved by reducing the contact temperature of metal to the liquidus line (~1180 °C for ferromaganese 85 % Mn, 1 % C, 0.80 % Si) when diffusion processes and kinetics of the reactions is slowing down.

The task consists in finding such a combination of layers of refractory materials that would provide the temperature of the highest magnesite layer of 1180 °C, when the lining corrosion will be calculated at ~0.20 cm/h (approximately 30 % lower) under other identical conditions. This can be reached by two lining zones made of fireclay and magnesite/dolomite (Table 2). At the lining temperature being 1180 °C and metal being 1350 °C, the expected heat flux will be (1350–1180)·18 = 3060 W/m$^2$, which is ~2 times higher than in the initial case for the temperature $t_{cm} = 1262$ °C (Table 1), but ~ 5 times lower than in the lining of magnesium and carbon material according to [6]. The results of the calculations are shown in Table 2 (it should be noted that for the furnace (Figure 1), the total lining height is greater than in [6].

Thus, it can be stated that the results of [6] are unbalanced and have differences between the data in figures and in the text. Replacement of a refractory material with another having a higher thermal conductivity (by 3–5 times) can never lead to a lower casing temperature at an elevated heat flux. It is probable that in the experiments of [6], an intense forced cooling of the casing was used for the furnace, but this was not shown clearly.

The overall optimization algorithm for the lining can be used in a rather simple way: the temperature of the upper layer of the lining should be maintained close to the liqui-

**Table 2.** Lining parameters in different variants

| Index | Work [6] | | Data of this work | |
|---|---|---|---|---|
| Height of layers of materials, m: | | | | |
| ● sintered magnesite | 0.585 | 0.285 | 0.983 | – |
| ● sintered dolomite | – | – | – | 0.906 |
| ● magnesium-carbon brick | – | 0.30 | – | – |
| ● fireclay brick | – | – | 0.067 | 0.144 |
| Temperature across the central axis of the furnace, °C: | | | | |
| ● outer casing ($t_c$) | 196 | 950* | 340 | |
| ● casing in contact with metal ($t_{cm}$) | 1262 | 1180 | 1180 | |

*Calculated by the heat transfer equation (1); in [6] 150 °C is shown.

dus temperature of the metal, which will allow delayering the rate of corrosion processes regardless of their mechanisms [6, 9]. Based on the known temperature of the metal, its liquidus temperature and heat transfer coefficients, the total heat flux is first estimated through the lining and the corresponding thermal resistance and the casing temperature, then the combination of layers of refractory materials is calculated, which will be optimal for these conditions. If the casing temperature is higher than the optimum, forced cooling can be attracted and the possibility of efficient disposal of thermal losses can be evaluated.

## CONCLUSIONS

1. The thermal mode of the furnace for ferromanganese production is important not only for the melting process, but also for the lining stability. The corrosion of a magnesite lining depends on the content of silicon in ferromanganese, temperature and convection of the metal, geometry and composition of the lining.

2. The analysis showed that the data of [6] regarding thermal mode of the lining operation exhibit inconsistence between the values of heat flux, heat transfer coefficients and limit temperatures. New calculations in this work showed that there should be a considered approach to replacing lining layers with other having higher thermal conductivity in order to prevent a high casing temperature and a possible freezing of the metal.

3. A convenient algorithm for optimization of the layers height and the composition of refractory lining materials was proposed to reduce the corrosion rate by maintaining the temperature of the upper layer of the lining close to the liquidus temperature of the metal of a particular composition.

## REFERENCES


1. Gasik, M.I. (1992) *Manganese*. Moscow, Metallurgiya [in Russian].
2. Gavrilov, V.A., Gasik, M.I. (2001) *Silicothermy of manganese*. Dniepropetrovsk, Sistemnye Tekhnologii [in Russian].
3. Gladkikh, V.A., Gasik, M.I., Ovcharuk, A.M., Projdak, Yu.S. (2007) *Ferroalloys furnaces*. Dniepropetrovsk, Sistemnye Tekhnologii [in Russian].
4. Gasik, M.I., Lyakishev, M.P., Gasik, M.M. (2009) *Physical chemistry and technologies of electric ferroalloys*. Dnipropetrovsk, Systemni Tekhnologii [in Ukrainian].
5. Gasik, M.M., Gasik, M.I., Shuvaev, S.P. (2018) Effect of high alkali content in ferrosilicomanganese smelting slags on slag properties and on the destruction of furnace lining. In: *Proc. of Congress INFACON XV, Cape Town, South Africa*. Vol. 2. Southern African Institute of Mining and Metallurgy, 307–313.
6. Parra, R., Mochon, J., Martin, D.R. et al. (2009) Bottom design optimization of electric arc furnace for ferromanganese production using nodal wear model. *Ironmaking and Steelmaking*, **36**, 529–536.
7. Lindstad, L.H., Aursjo, S. (2018) Monolithic furnace linings for production of ferro-alloys. In: *Proc. of Congress INFACON XV, Cape Town, South Africa*. Vol. 2. Southern African Institute of Mining and Metallurgy, 259–268.
8. (1980) *Electrothermal equipment:* Handbook. Ed. by A.P. Altgausen. Moscow, Energiya [in Russian].
9. Wang, S., Jin, Y., Li, G. (2004) Theory and application of magnesia ramming material in ferroalloy refining furnaces. In: *Proc. of Congress INFACON X, Cape Town, South Africa*. Southern African Institute of Mining and Metallurgy, 735–740.


## ORCID

M.M. Gasik: 0000-0002-5782-7987

## CORRESPONDING AUTHOR

M.M. Gasik
Aalto University, 00076 AALTO, Espoo, Finland.
E-mail: michael.gasik@aalto.fi

## SUGGESTED CITATION

M.M. Gasik (2024) Optimization of the refractory lining for ferromanganese production furnace. *The Paton Welding J.*, **7**, 35–38.
DOI: https://doi.org/10.37434/tpwj2024.07.06

## JOURNAL HOME PAGE

https://patonpublishinghouse.com/eng/journals/tpwj

Received: 18.02.2024
Received in revised form: 10.05.2024
Accepted: 09.07.2024

DOI: https://doi.org/10.37434/tpwj2024.07.07

# DEVELOPMENT OF THE TECHNOLOGY OF FERRONICKEL PRODUCTION IN UKRAINE

**D.V. Shevchenko[1], S.V. Prykhodko[1], A.A. Nadtochii[2], V.Yu. Shutov[3], A.M. Ovcharuk[2]**

[1]Pobuzky Ferronickel Plant
12 Promyslova Str., Pobuzke village, Golovanivsky district, Kirovohrad region, 26555, Ukraine
[2]Ukrainian State University of Science and Technology
4 Nauky Prosp., 49600, Dnipro, Ukraine
[3]National Technical University "Dnipro Polytechnic"
19 Dmytro Yavornytskyi Prosp., 49005, Dnipro, Ukraine

**ABSTRACT**

The paper summarizes the results of numerous works performed by the employees of the Pobuzky Ferronickel Plant, the Department of Electrometallurgy of the USU of Science and Technology (Dnipro), RPC "Technosplavy" under the leadership of Mykhailo Hasyk, academician of NASU. A technology of low iron recovery has been implemented at the plant, which allows producing high-percentage black ferronickel, containing 30–50 % Ni, and almost hundredth fractions of carbon and silicon, directly in electric furnaces. The thermodynamic features of out-of-furnace ladle desulfurization of ferronickel with soda are considered. A complex technology has been developed and implemented, which involves mixing black ferronickel with a reduced silicon and carbon content (up to 0.01 %) and a high nickel content (over 50 %) produced in one furnace with an alloy from another furnace with a low nickel concentration (10–17 %) and a high concentration of silicon and carbon, which are so necessary for desulfurization with soda in a ladle. The developed and proposed technological schemes for the enrichment of electric furnace slags using the "wet" technology and refining slags using the "dry" technology make it possible to recycle about 1,200 tons of nickel per year, or to extract 31.6 % and 94.65 % of nickel from the slags, respectively.

**KEYWORDS:** Pobuzky Ferronickel Plant, cinder, black ferronickel, ladle desulfurization, refining, slag enrichment

## INTRODUCTION

Pobuzky Ferronickel Plant (PFP), which in 2022 celebrated its half a century jubilee, was put into operation for processing low-quality (up to 1 % Ni) local iron-silicon nickel ores of Kapitanivka deposit (Ukraine, Kirovohrad region). Ferronickel produced at the Plant, was characterized by an increased content of impurities (Si, Cr and C) in the black metal. So, silicon content in ferronickel in some melts was higher than nickel content, reaching the values of 6–8 % [1]. More over, the need to use fluxing additives, led to higher power consumption, increase of the amount of slag and respective nickel losses [2, 3]. After PFP restart (2001), it became possible to fundamentally change the approach to ferronickel production, which corresponds to current market requirements to nickel-containing products. The base of this concept was application of imported ore rich in nickel, and transition to melting of commercial ferronickel with up to 25 % nickel content [4, 5]. The ore was supplied from New Caledonia and Indonesia. In connection with the fact that Indonesia stopped ore export from the beginning of 2014, PFP switched over to Guatemalan ore, which is characterized by higher content of nickel and magnesium oxide (Table 1), compared to ore from Kapitanivka deposit [5], on the base of which the Plant was designed and operated till 2006.

Over the long period of operation, the Plant developed and introduced many innovations into production [6–11], that ensured the high production efficiency. The most significant of them are energy carriers for cinder preparation in tubular rotary furnaces (TRF) from fuel oil through natural gas to pulverized coal fuel (PCF), ore predrying (from 35–38 to 20–23 %) of moisture for PCF, granulation of commercial ferronickel, installation of ore-recovery furnace (RVP1) of HATCH Company, Canada, that allows increase the capacity of the used furnace power, and lining service life due to its damping.

Recently, the technology of low iron recovery (TLIR) has been introduced at the plant, which allows

**Table 1.** Chemical composition of ores from different deposits, wt.%

| Deposit | Ni | Fe | $SiO_2$ | CaO | MgO | $Cr_2O_3$ | $Al_2O_3$ |
|---|---|---|---|---|---|---|---|
| Kapitanivka (Ukraine) (1972–2001 pp.) | 0.8 | 16 | 38.5 | 17 | 4.8 | 3.5 | 2.9 |
| New Caledonia (2001–2006 pp.) | 2.22 | 14.89 | 38.77 | 1.11 | 20.60 | 1.66 | 1.74 |
| Indonesia (2006–2012 pp.) | 2.08 | 12.62 | 42.95 | 1.05 | 21.45 | 1.18 | 1.91 |
| Guatemala (TLRI) (2013–2016 pp.) | 1.88 | 15.66 | 34.8 | 1.23 | 22.0 | 0.98 | 2.7 |

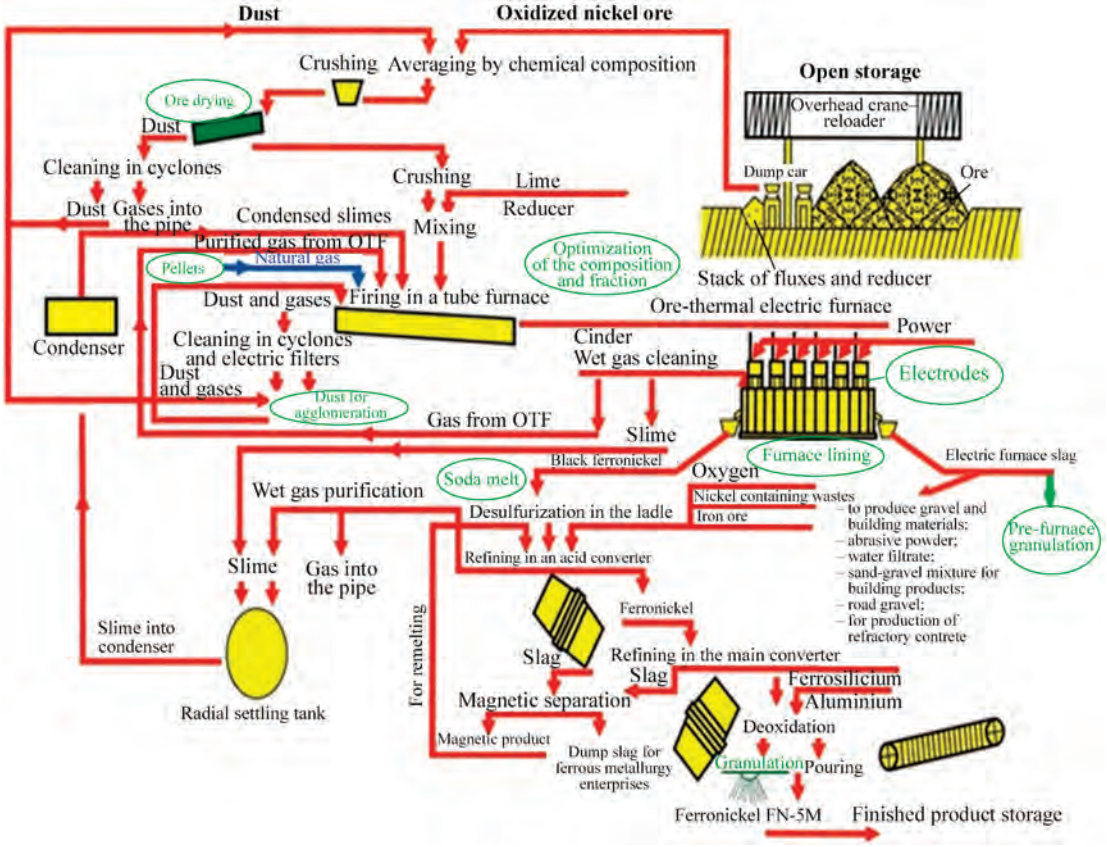


**Figure 1.** Acting technology scheme of ferronickel production at PFP [12]

producing directly in electric furnaces a high-percentage black nickel, containing 30–50 % Ni and practically hundredth fractions of carbon and silicon (0.02 and 0.01 %, respectively), which influence desulfurization of black ferronickel with soda in the ladle.

The technology scheme of ferronickel production in electric furnaces includes the following stages [12, 13] (Figure 1): preparation and averaging of nickel-containing ore in an open storage; ore drying, charge material dosing and roasting of the charge, consisting of ore, limestone, anthracite and back dust, in tubular rotary furnaces; electric melting of black ferronickel in ore-thermal furnaces (RTP-1 and RPT-2) using hot charge (cinder) from tubular rotary furnaces, refining of a mixture of black ferronickel from two furnaces by the methods of out-of-furnace desulfurization of the melt in the ladle with soda ash or soda melt; successive refining of black ferronickel from silicon, chromium, carbon, sulfur and phosphorus in converters with acid and basic lining with upper oxygen blowing (duplex-process); pouring refined ferronickel in conveyor-type filling machines or water granulation; release and granulation of electric furnace slag, which is disposed as construction gravel and abrasive materials.

Charge for firing in drum furnaces consists of the following components: 1 t of dry ore; 352 kg of limestone; 106 kg of anthracite coal and 5 kg of back dust. The furnace diameter is 3 m and length is 75 m. The firing zone in the furnace is 9–12 m. The fuel used is pulverized coal fuel (PCF) [14, 15]. The flame temperature reaches 1200 °C, and the charge is heated to not more than 850 °C, to avoid overheating and formation of ring deposits. The furnaces operate on counterflow principle. The duration of material staying in TRF is 1.5–2.0 h.

The process of firing in tubular rotary furnaces is divided into three zones: drying; heating; and firing. In the drying zone, starting from the loading end of the furnace, the raw material is heated up to 120 °C with removal of free (hygroscopic) moisture. In the heating zone the raw material is heated up to 700–800 °C with partial removal of crystallization moisture, present in the composition of mineral compounds. In the firing zone the raw material is heated up to 900–1000 °C. This process is accompanied by decomposition and partial reduction of nonferrous metal oxides, and higher iron oxides to oxide and removal of crystallization moisture.

During firing the temperature should be in the range of 950–1000 °C, evolving gases temperature should be not lower than 420 °C, the amount of gases released from TRF is up to 55000 $m^3$/h. The gas composition here changes in the following ranges, %: $CO_2$ — 5–15, $O_2$ — 2–5; CO — absent; $N_2$ — balance.

Reduction electric melt of nickel ore to produce ferronickel consists of 65–85 % slag from the loaded cinder and 10–18 % of black ferronickel.

Two ore-smelting (three-phase, six-electrode) AC electric furnaces of installed power of 48 MV.A are operating at Pobuzky Ferronickel Plant. Electrode diameter is 1200 mm, distance between electrode axes is 3200 mm; electrodes are located vertically, suspended from three hydraulic cylinders, which ensure electrode travel (along the vertical) of 1400 mm. The electrodes are continuous self-sintering.

Electric melting is performed using cinder with 600–700 °C temperature of the following composition, %: 0.7–0.9 Ni; 0.03–0.05 Co; 15–18 Fe; 45–36 $SiO_2$; 16–20 CaO; 4–6 MgO. Cinder reduction proceeds due to the use of carbon of anthracite of AC grade or culm of ASh grade, thermal coal and silicon-carbide material [15].

During reduction melting, iron and nickel pass from the oxide melt into metal phase. Part of the nickel oxides interacts with silica from silicates of 2 (Fe, Ni)O·$SiO_2$ type and forms nickel silicates [16, 17].

In Ni–O–Si system one compound 2NiO·$SiO_2$, nickel orthosilicate, is crystallized, which at the temperature of about 750 °C can be reduced with carbon by the following reaction

$$(2NiO{\cdot}SiO_2) + 2C = 2[Ni] + (SiO_2) + 2CO.$$

At 900–1100 °C $CO_2$ content in the gas phase is equal to 60–75 %. Nickel dissolution in iron occurs by the following reactions

$$(2FeO{\cdot}SiO_2) + C = 2[Fe] + (SiO_2) + 2CO,$$
$$[Ni] + [Fe] = [Ni]_{Fe}$$

and it promotes process recovery. Phosphorus and sulfur easily transform into the metal phase — ferronickel.

Special attention should be given to silicon and carbon content, the concentration of which determines the metal temperature and solubility of the latter in it. Silicon has the strongest influence on carbon solubility in black ferronickel. Increase of silicon content lowers the equilibrium concentration of carbon dissolved in black ferronickel.

Optimal silicon content in black ferronickel is 3–4 % [7]. Here, the process of out-of-furnace desulfurization is more complete. Lowering of silicon content impairs the indices of further ferronickel refining process. Higher silicon content leads to the need to increase the consumption of cooling additives during conversion.

As black ferronickel contains a large amount of sulfur, which enters the melt with carbon reducing agent and ore, it is subjected to out-of-furnace ladle desulfurization with soda (sodium carbonate) [13, 17, 18]. It yields ferronickel corresponding to FN-6 grade by its composition, which is used in foundry. The process of sulfur removal can be generalized by the following reaction:

$$[S]_{Fe-Ni} + 2(Na_2CO_3) + [C] + [Si] = (Na_2SiO_3) + 3CO + (Na_2S).$$

Temperature dependencies of Gibbs free energies of the possible reactions of sulfur interaction with soda are given below:

$$FeS + 3Na_2CO_3 + 2Si = 2Na_2SiO_3 + Na_2S + Fe + 3CO,\ \Delta G_T^0 = -326578 + 430\,T,\ \text{kJ/mol}; \quad (1)$$

$$NiS + 3Na_2CO_3 + 2Si = 2Na_2SiO_3 + Na_2S + Ni + 3CO,\ \Delta G_T^0 = -340447 + 440\,T,\ \text{kJ/mol}; \quad (2)$$

$$FeS + Na_2CO_3 + C = Fe + Na_2S + CO + CO_2,\ \Delta G_T^0 = -362121 + 330\,T,\ \text{kJ/mol}; \quad (3)$$

$$NiS + Na_2CO_3 + C = Ni + Na_2S + CO + CO_2,\ \Delta G_T^0 = -348251 + 340\,T,\ \text{kJ/mol}; \quad (4)$$

$$FeS + 3/2Na_2CO_3 + 1/2Si + 3/2C = 1/2Na_2SiO_3 + Na_2S + Fe + 3CO,\ \Delta G_T^0 = -317508 + 485.5T,\ \text{kJ/mol}; \quad (5)$$

$$NiS + 3/2Na_2CO_3 + 1/2Si + 3/2C = 1/2Na_2SiO_3 + Na_2S + 2Ni + 3CO,\ \Delta G_T^0 = -305138 + 495\,T,\ \text{kJ/mol}. \quad (6)$$

Analysis of the derived results shows that compared to carbon, silicon has a thermodynamically more effective influence on desulfurization in the system (Figure 2), although some production specialists note that it is exactly carbon, which has the strongest influence on desulfurization process, that is probably related to the kinetic parameters of the process – influence of the gas phase (CO content) on reagent stirring and increase of their contact surface.

Equilibrium phase distribution in 0.5FeS + 0.5NiS + 3$Na_2CO_3$ system was determined using HSC Chemistry 6.0 Program data base, which was developed by the specialists of Research Center of Outotec Company.

The process of intensive desulfurization of nickel sulfide starts at the temperature of 500 °C and is over at approximately 1000 °C, and that of iron sulfide – at 750 and 1250–1350 °C, respectively. Degree of nickel desulfurization with soda is equal to 94–96 %, that of iron is 60 %, and with process temperature increase above 1350 °C its resulfurization is possible.

Equilibrium phase distribution in the complex system of FeS–NiS–$Na_2CO_3$–C–Si allowed determination of the optimal temperature mode of ladle desulfurization of ferronickel with soda, which is in the range of 1300–1350 °C.

During ferronickel desulfurization (0.13–0.40 % S) in the ladle with soda (consumption of 4–5 % of the metal weight) the degree of desulfurization is equal to 50–60 %, and the minimal sulfur content at the level of 0.048 % is reached in practice. To ensure the high

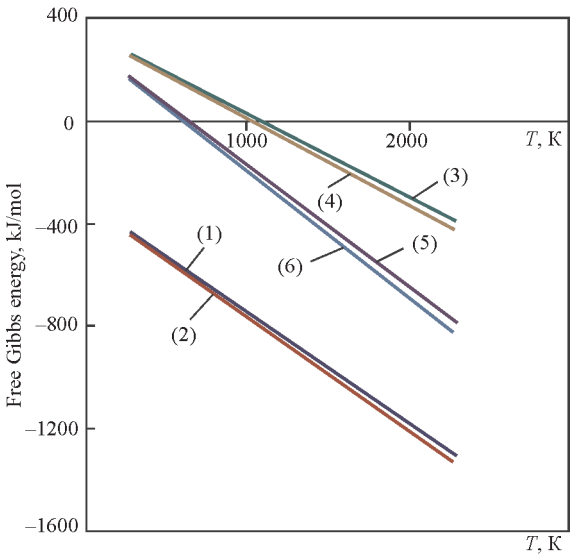


**Figure 2.** Free Gibbs energy for possible reactions (1)–(6) of sulfur interaction with soda

efficiency of desulfurization with soda in the ladle, it is necessary to eliminate the possibility of electric furnace slag ingress at metal release, as soda interaction with silicon dioxide and $Na_2SiO_3$ formation lead to its considerable losses that requires repeated metal processing by this scheme after loading the soda slag.

Chemical composition of black ferronickel, depending on the quality of nickel-containing raw materials from different deposits, is given in Table 2.

After commissioning of RTP-1 of HATCH Company, Canada, and introduction of the technology of low iron reduction (TLIR), it became possible to produce ferronickel, which contains only hundredth fractions of a percent of silicon and carbon that eliminates the possibility of its out-of-furnace refining with soda. Here, sulfur content increased two times, and was equal to 0.2–0.5 %, and electrode mass consumption was significantly increased.

That is why, the Plant developed and introduced a comprehensive technology, which envisages mixing black ferronickel, released from RTP-1 with a lower content of silicon and carbon (to 0.01 %) and high Ni content (higher than 50 %) with an alloy from RTP-2 with a low concentration of nickel (10–17 %) and high concentration of silicon and carbon, so necessary for soda desulfurization in the ladle.

Mixing allowed returning to project technology – out-of-furnace desulfurization with calcinated soda in a ladle and finishing metal in the ladle. At present the technology of low reduction of iron has been mastered at Pobuzky Ferronickel Plant in RTP-1. Here, nickel content in black ferronickel increased up to 50 %, and silicon and carbon content was equal to only 0.01 % that makes the process of ladle desulfurization with soda more complicated.

Soda slag, forming during out-of-furnace desulfurization, is thoroughly scraped from the metal surface in the amount of 350–600 kg with wooden scrapers into a technological bowl, specially designated for this purpose. After desulfurization before pouring into acid converter the weight of black ferronickel, remaining in the ladle, with part of the soda slag, changes in the range of 34.95–37.80 t of the following composite, %: 14.1–15.5 Ni; 0.23–0.26 Co; 3.3–3.7 Si; 0.045–0.073 S; 1.4–15 Cr; 2.4–2.6 C; 0.093–0.1 P; 0.052–0.059 Cu, the temperature of which varies in the range of 1200 to 1250 °C.

Comparative analysis of technical indices of the process of black ferronickel refining by the three schemes (Table 3) shows that the most efficient is the project technology, by which both the furnaces are operating for complete reduction. Analyzing the indices of RTP-1 and RTP-2 operation by the technology of melt mixing at release from the furnace, it should be noted that RTP-2 operates more efficiently in production of black ferronickel, as over the same operation period at Ni content of 45.22 % in the alloy in the first furnace its release is by 34 % less, than in the other furnace with 10.53 % Ni content.

Black nickel refining by the experimental technology required increasing the consumption of ferrosilicium, additionally using aluminium and lime. The melting time is increased by 26 and 40 %, respectively, compared to the mixing and project technology, and process productivity is also decreased considerably by 52.2 and 60 %, respectively.

Comparison of specific material consumption for refining and removal of 1 kg of sulfur again confirmed the higher efficiency of project scheme (Table 4), which is based on desulfurization of nickel cast iron.

Ferronickel partially cleaned from sulfur, is poured into the converter with acid fire-resistant lining and it is subjected to oxygen blowing to remove silicon and chromium [19].

**Table 2.** Chemical composition of black ferronickel, melted using raw materials from different deposits, wt.%

| Deposit | Ni | Si | Cr | C | S | P |
|---|---|---|---|---|---|---|
| Ukraine | 7.86 | 4.79 | 2.80 | 3.50 | 0.35 | 0.012 |
| New Caledonia | 16.89 | 1.93 | 1.29 | 2.84 | 0.30 | 0.020 |
| Indonesia | 18.51 | 4.02 | 1.53 | 2.55 | 0.26 | 0.0313 |
| Guatemala (old technology) | 13.41 | 3.41 | 2.11 | 2.79 | 0.17 | 0.053 |
| Guatemala (TLIR) | 37.30 | 0.01 | 0.04 | 0.03 | 0.48 | 0.064 |

**Table 3.** Technical indices of out-of-furnace desulfurization of black ferronickel by different technology schemes

| Parameter | Technology schemes | | | |
|---|---|---|---|---|
| | Experimental (01.11.2020–09.02.2021) | Mixing | | Project |
| | | RTP-1 | RTP-2 | |
| Black ferronickel, t | 3341.6 | 1022.1 | 5889.25 | 10525 |
| Nickel, t | 1406.8 | 462.55 | 619.6 | 1418 |
| Ni content, % | 42.1 | 45.22 | 10.53 | 13.48 |
| S content, t | 0.283 | 0.36 | 0.089 | 0.298 |
| $CaCo_3$ consumption, t | 48.0 | 805.5 | | 305 |
| FeSi consumption, t | 70.0 | 18.56 | | 48.15 |
| Soda consumption, t | 87.17 | 73.85 | | 117.7 |
| Al consumption, t | 13.75 | – | | – |
| Lime consumption, t | 239.0 | – | | Fe ore 79 |
| Melting time, h | 2.15 | 1.7 | | 0.70/0.84 |
| $O_2$ blowing, min | 20.6 | 21.64 | | 8.12/15.21 |
| $O_2$ flow rate, $nm^3$ | 228630 | 194402/286645 | | 320058/107991 |
| Produced | | | | |
| Commercial FeNi, t | 2600 | 5920 | | 9130 |
| Nickel, t | 1521 | 1119.6 | | 1584 |
| Ni content, % | 54.53 | 18.9 | | 17.4 |
| Ni removal, % | 92.4 | 95.9 | | 96.6 |
| S content, % | 0.059 | 0.043 | | 0.068 |
| Slag ratio | 0.60 | 0.40 | | 0.26 |
| Nickel in slag, % | 0.52 | 0.19/0.14 | | 0.180/0.226 |
| Sulfur removal, t | 0.792 | 0.635 | | 2.516 |

The finished alloy is poured in conveyor machines. Product weight is 40–50 kg. Slag from the main conversion has the following composition, %: CaO — 15–20; $SiO_2$ — 5–10; FeO — 35–50; Ni — 0.05; Co — 0.005; $Cr_2O_3$ — 1–10.

Slags from acid and basic conversion are subjected to magnetic separation to extract ferronickel particles. Specific power consumption for metallurgical processing of 1 t of dry nickel-containing ore is equal to 810 kW·h/t, or 78200 kW·h per 1 t of nickel. The processes of refining black ferronickel in acid and basic converters allow producing commercial alloy, meeting the requirements of world standards.

Production of ferronickel from oxidized nickel ores is based on application of raw materials, where nickel content is practically not higher than 2.5 %, so that the process is characterized by a large volume of slag, the ratio of which is 6–10 units, and it is the highest in ferroalloy electrothermy.

The most important aspect of recycling ferroalloy slags is their separation into the oxide and metal phases, the content of which is higher than 10 % in some cases.

Nowadays different methods of separation of the metal and oxide components of the slags are applied in the world practice, starting from manual selection up to modern X-ray radiometric separation, although technologies based on gravity and magnetic processes became the most widely accepted.

Based on the results of studying the samples of electric furnace and refining slags from ferronickel production using oxidized nickel ore from the Guatemala deposit, the method of X-ray spectral microanalysis (XSMA) analysis performed in Selmi PEM-1061 unit was applied to determine that the main amount of nickel is concentrated in metal phase shot of different shape in compounds with iron and sulfur, the concentration of which is up to 70 % in some cases. No nickel was found in the oxide phase of the slags, and it is probably contained in microshot.

**Table 4.** Material consumption for refining and desulfurization of black ferronickel, kg/kg of sulfur

| Material | FeNi production schemes | | |
|---|---|---|---|
| | Experimental | Mixing | Project |
| Soda ash | 110 | 116 | 44 |
| Limestone | 61 | 267 | 121 |
| Ferrosilicium | 88.4 | 29.2 | 19.14 |
| Aluminium | 17.4 | – | – |
| Lime | 301 | – | – |
| Oxygen, $nm^3$ | 288 | 757 | 170 |

The studied high-manganese (31.5–34.7 % MgO) acid ($CaO + MgO_2/SiO_2 = 0.72–0.74$) electric furnace granulated slags from ferronickel production, containing up to 0.31 % Ni, are represented by 0.5–5.0 mm fraction by more than 95 %, and refining highly basic ($(CaO + MgO)/SiO_2$ higher than 3.0), which are self-disintegrating, with nickel concentration from 9.3 up to 10.95 %, are represented by less than 0,5 mm fraction practically by 40 %.

Based on investigation of the features of initial raw material and its movement in the working zones of separation units, a new method was developed for ferroalloy slag enrichment, both by gravity separation method, and by wet method using an upgraded magnetic separator, adapted to the characteristics of the initial raw material, which allowed increasing the indices of nickel extraction from electric furnace slags.

The schematic of refining slag processing (Figure 3) envisages feeding slag crushed in the ball mill, into gravity separator, where its separation into size grades takes place. The material of 0.4–1.6 and + 1.6 mm size fractions is fed to the magnetic separator, where it is separated into the magnetic (metal) and nonmagnetic (slag) fractions.

Performed studies of slag enrichability in ferronickel production by the developed technology scheme allowed producing from them metal concentrate, containing 0.9–4.75 % nickel with the yield of 2–5 % of initial raw materials.

Performed studies on the classification and enrichment of the refining slags showed that slag fraction larger than + 1.6 mm contains 38 % of nickel at its yield of 10–14 %, and in the size grades from 0.16 up to 1.6 mm with the total yield of 43.6 % nickel content is equal to 21.94 %. In dump refining slags nickel content is not higher than 0.5 % that is 18.6–21.9 times lower than in the initial material.

The developed and proposed for introduction technology schemes of enrichment of electric furnace slags by the wet technology and of refining slags by the dry technology allow recycling close to 1200 t of nickel per year, or extracting 31.6 and 94.65 % nickel from the slags, respectively. At the world price of nickel of 18525 USD, formed by the end of 2021, the total cost effect will be equal to 22.23 mln USD.

Thus, the limited scope of the journal paper does not allow fully disclosing all the innovations and developments, performed by the staff of Electrometallurgy Department of the Ukrainian state University of Science and Technologies under the leadership of M.I. Gasik and introduced at the Plant with the assistance of scientific-technical staff and its management, many of whom are the graduates of this Department, which enabled the Plant to joint the TOP-5 of enterprises of the metallurgical complex of Ukraine on currency earnings, and the parameters of its electrothermal equipment and electrotechnological modes

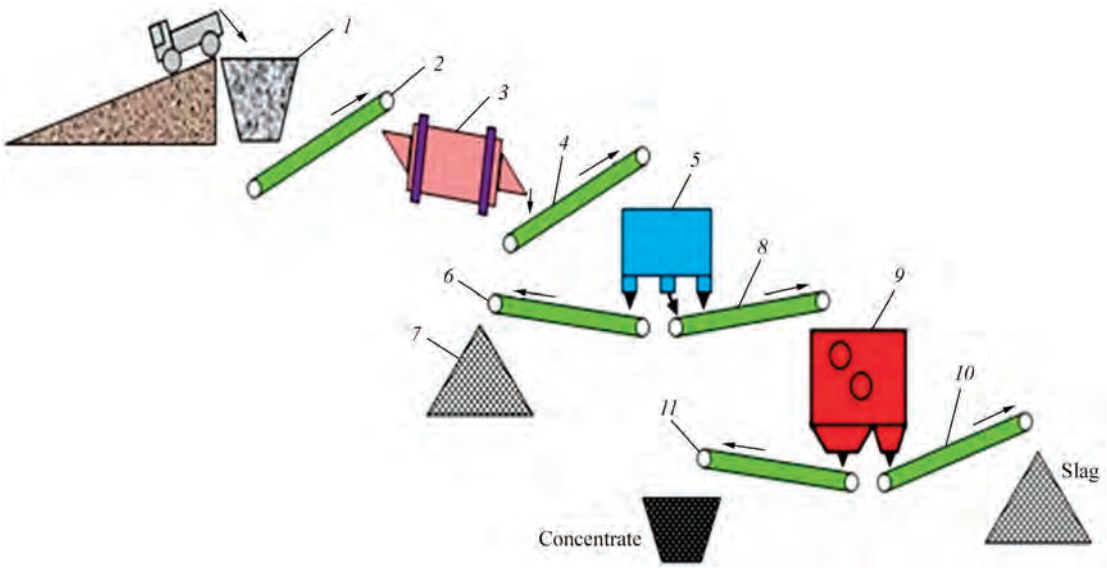


**Figure 3.** Technological line for processing refining slags: *1* — receiving hopper with feeder; *2, 4, 6, 8, 10, 11* — belt conveyors; *3* — ball mill; *5* — gravity separator; *7* — fraction stacking (0.16 mm); *9* — magnetic separator

of its operation were incorporated in the construction of enterprises by foreign SinoSteel Group Co (China) and Solvij (Indonesia) Companies.

## REFERENCES


1. Gasik, M.I., Lyakishev, M.P. (2009) *Physics-chemistry and technology of ferroalloys:* Manual. 3rd Ed. Dnipro, Systemni Tekhnologii [in Ukrainian].
2. Sokolov, K.D., Kapran, I.I., Likhachev, V.F. (2000) Examination of lining operation of ore-thermal furnaces in melting of ferronickel. *Metallurgicheskaya i Gornorudnaya Promyshlennost*, **6**, 32–35 [in Russian].
3. Novikov, N.V., Kapran, I.I., Sokolov, K.D. et al. (2006) Petrographic examinations of interaction of periclase-chromium lining of ore-smelting furnace with melt of ferronickel and furnace slag. *Metallurgicheskaya i Gornorudnaya Promyshlennost*, **2**, 27–30 [in Russian].
4. Novikov, N.V., Sokolov, K.D., Kapran, I.I., Ovcharuk, A.N. (2005) Material balance of process of ferronickel production. *Metallurgicheskaya i Gornorudnaya Promyshlennost*, **4**, 20–24 [in Russian].
5. Novikov, N.V., Sokolov, K.D., Kapran, I.I., Ovcharuk, A.N. (2005) Examination of chemical, mineralogical and phase composition of nickel ore for ferronickel melting. *Metallurgicheskaya i Gornorudnaya Promyshlennost*, **5**, 19–22 [in Russian].
6. Bespalov, O.L., Sokolov, K.D., Prikhodko, S.V. et al. (2017) State-of-the-art and prospects of improvement of ferronickel production technology. In: *Current problems of development of metallurgical science and education*, 204–211 [in Russian].
7. Gasik, M.I., Zaporozhets, B.O., Novykov, M.V. et al. (2011) *Method of melting of roughing ferronickel with optimal silicon content.* Pat. 62847, Ukraine, Int. Cl. C 22 B 23/00 [in Ukrainian].
8. Gasik, M.I., Zaporozhets, B.O., Kapran, I.I. et al. (2004) *Start section of self-sintering electrode.* Pat. 2852, Int. Cl. H05B7/09 C21B11/10 C01B31/02 [in Ukrainian].
9. Gasik, M.I., Kapran, I.I., Kashkul, V.V. et al. (2004) *Method of initial sintering of self-sintering electrode.* Pat. 2854, Ukraine. Int. Cl. C01B31/02 H05B7/09 [in Ukrainian].
10. Bespalov, O.L., Prykhodko, S.V., Danov, O.V. et al. (2016) *Reducing mixture for electrothermal ferronickel production.* Pat. 109001, Ukraine. Int. Cl. C22 B 4/06 [in Ukrainian].
11. Bespalov, O.L., Mashiyanov, V.G., Solokha, V.K. et al. (2018) *Unit for metal refining.* Pat. 120548, Ukraine. Int. Cl. B22D1/00 C21C7/072 C21C1/00 C21C7/00 C22B9/05 C22B9/20 [in Ukrainian].
12. Bezugliy, A.V., Nikolenko, A.V., Shevchenko, D.V. et al. (2021) Improvement of the process of conducting arc-free ferronickel melting in a six-electrode furnace. In: *Proc. of the 16th Int. Ferro-Alloys Congress (INFACON XVI) 2021, 27–29 September 2021*. https://ssrn.com/abstract=3929902 or http://dx.doi.org/10.2139/ssrn.3929902
13. Novikov, N.V., Kapran, I.I., Sokolov, K.D. et al. (2006) Innovative technological processes of electric furnace ferronickel refining by progressive industrial methods. Information 2. Thermodynamic investigations of processes and technology of ladle desulfuration of electric furnace ferronickel by sodium carbonate. *Advances in Electrometallurgy*, **2**, 36–39.
14. Melnik, S., Akreev, V., Prykhodko, S. et al. (2023) Degree of solid-phase reducing of iron from nickel ore oxides in tubular rotary furnace using thermal grade-coal as reducing agents. *Modern Engineering and Innovative Technologies*,1(29-01), 87–95. DOI: https://doi.org/10.30890/2567-5273.2023-29-01-069
15. Prykhodko, S., Shevchenko, D., Akreev, V. et al. (2023) Melting of complex laterite ores and selection of optimal reducing agents. *Modern Eng. and Innovative Technologies*, 1(29-01), 61–70. DOI: https://doi.org/10.30890/2567-5273.2023-29-01-067
16. Novikov, N.V., Kapran, I.I., Sokolov, K.D. et al. (2006) Innovation technological processes of electric furnace ferronickel refining by progressive industrial nethods. Pt 1. Thermodynamic properties of nickel-base systems and binary compounds. *Advances in Electrometallurgy*, **1**, 36–40.
17. Novikov, N.V., Kapran, I.I., Sokolov, K.D. et al. (2006) Innovative technological processes of electric furnace ferronickel refining by progressive industrial methods. Pt 3. Processes and technology for refining ferronickel in acid and basic oxygen converters. *Advances in Electrometallurgy*, **3**, 41–44.
18. Shevchenko, D.V., Zamkovoy, O.V., Ovcharuk, A.N. et al. (2021) Thermodynamic model of the process of desulfurization of a black ferronickel in a ladle. In: *Proc. of the 16th Int. Ferro-Alloys Congress (INFACON XVI) 2021, 27–29 September 2021*. https://ssrn.com/abstract=3930143 or DOI: http://dx.doi.org/10.2139/ssrn.3930143
19. Ovcharuk, A., Akreev, V., Prykhodko, S., Melnyk, S. (2023) Blowing of converter bath in ferronickel refining using one-nozzle and three-nozzle tuyeres. *Modern Eng. and Innovative Technologies*, 1(29-01), 71–86. DOI: https://doi.org/10.30890/2567-5273.2023-29-01-068


## ORCID


D.V. Shevchenko: 0009-0006-5147-0151,
S.V. Prykhodko: 0009-0005-0013-2198,
A.A. Nadtochii: 0000-0001-5077-0562,
A.M. Ovcharuk: 0009-0007-0218-2513


## CONFLICT OF INTEREST

The Authors declare no conflict of interest

## CORRESPONDING AUTHOR


D.V. Shevchenko
Pobuzky Ferronickel Plant
12 Promyslova Str., Pobuzke village, Golovanivsky district, Kirovohrad region, 26555, Ukraine.
E-mail: office@pfk.com.ua


## SUGGESTED CITATION


D.V. Shevchenko, S.V. Prykhodko, A.A. Nadtochii, V.Yu. Shutov, A.M. Ovcharuk (2024)
Development of the technology of ferronickel production in Ukraine. *The Paton Welding J.*, **7**, 39–45.
DOI: https://doi.org/10.37434/tpwj2024.07.07


## JOURNAL HOME PAGE

https://patonpublishinghouse.com/eng/journals/tpwj


Received: 07.04.2024
Received in revised form: 03.06.2024
Accepted: 29.07.2024

# FUTURE TRENDS AND TECHNOLOGIES IN THE WELDING INDUSTRY: VISION OF DNIPROMETYZ TAS

The welding industry is on the verge of significant changes driven by new technologies and evolving market needs. DNIPROMETYZ TAS one of the leading manufacturers of welding wire in Ukraine, is actively adapting to these changes and offering innovative solutions.

## KEY MARKET DEVELOPMENT TRENDS

Recent trends in the development of the welding materials market predict significant growth over the next six years. Welding technologies are widely used to create metal structures in various sectors of the economy. Welding plays a crucial role in construction, bridge building, pipeline laying, and other engineering projects. The main drivers of this growth are the automotive and fuel and energy industries, which actively use welding technologies for manufacturing metal structures. The energy sector is likely to meet the growing demand for solar and wind power plants. Pipeline construction is also expected to support market growth over the next six years.

The main factors driving the growth of the welding materials market are industrialization, urbanization, and technological progress.

## MODERN CHALLENGES AND SOLUTIONS

The primary obstacles to market development are unstable raw material supplies and price fluctuations. Changes in trade regulations, supply imbalances, environmental requirements, currency fluctuations, and geopolitical threats significantly impact the cost of raw materials, negatively affecting the production and price of welding materials.

Industries related to the production of welding materials face a shortage of skilled welders due to the mass retirement of experienced workers. This has particularly affected sectors such as heavy engineering, automotive manufacturing, and construction, where welding technologies are most intensively used.

In response to this challenge, DNIPROMETYZ TAS actively collaborates with educational institutions, invests in the training of young specialists and provides consultations and technical assistance at all the stages: from material selection to product application.. The plant also actively collaborates with customers and focuses its efforts on user training, which strengthens our brand and creates strong partnerships.

Stable expansion of the welding materials market is expected in Europe, thanks to the already developed infrastructure. DNIPROMETYZ TAS is working on expanding the European market, particularly in Germany, whose economy is considered one of the strongest in Europe. The European Union is strengthening environmental protection measures, leading to an increase in the production of environmentally friendly products. This encourages the development of welding materials that will reduce pollution levels in the future.

Diversification of products and the introduction of new technologies are the main strategies for growth and development in the market.

## KEY SEGMENTS OF THE WELDING MATERIALS MARKET

Depending on the type of welding material, the market is divided into solid wire (38 %), flux-cored wire (27 %), coated electrodes for manual arc welding (26 %), and wire and fluxes for submerged arc welding (9 %).

The solid wire market segment maintains its leadership due to its broad application in various industries. This segment is expected to continue dominating, as solid wire is actively used for arc welding in inert gases. Its high productivity, efficiency, and ability to create clean and strong welds attract the attention of new market players.

The welding materials industry is currently focused on developing simple and economical solutions for protecting parts from the environment. To prevent oxidation, solid wire is copper-coated, which improves conductivity. However, copper is unsuitable for some types of welding, increasing the demand for polished wire with a high degree of surface cleanliness. Such wire is especially useful in robotic welding, but its supply on the market is still limited.

Coated electrodes for manual arc welding, mainly intended for low-alloy and low-carbon steels, remain popular due to their wide range of applications and availability.


The product range of DNIPROMETYZ TAS includes a wide variety of diameters of copper-coated welding wire, as well as polished, non-coated welding wire. Wires of the G3Si1 and G4Si1 grades are produced in accordance with the international standard EN ISO 14341 (national standard DSTU EN ISO 14341). The plant strives to offer not only welding materials but also comprehensive solutions, including application technologies for effective welding tasks. The goal is for our customers to see DNIPROMETYZ TAS not just as a supplier but as a strategic partner capable of solving their tasks.

## INNOVATIONS AND AUTOMATION

Automation and robotization of welding processes are becoming the foundation of the industry's future development. Robotic welding complexes significantly increase the productivity and quality of welding work, as well as reduce the risk of injuries. To fully meet the needs of its customers, DNIPROMETYZ TAS has expanded its range of welding wire by adding a new format — 250 kg drums for robotic systems. This product allows the automation of processes in large-scale production.

The plant uses advanced technologies from the Swedish manufacturer Lämneå Bruk AB and high-quality raw materials to produce welding wire. Quality control of the rod and testing of finished products are carried out in our own accredited laboratory, equipped with modern instruments for chemical analysis, mechanical tests, and welding technology tests. This ensures the production of the highest quality products, tested at leading industrial enterprises.

The integration of digital technologies with industrial processes is becoming increasingly important. The fourth industrial revolution, aimed at creating “smart” manufacturing, is already impacting the welding industry. DNIPROMETYZ TAS actively uses intelligent production management systems, which enhance its efficiency and flexibility, as well as improve customer orientation at all stages of production.

We pay special attention to certifying our products and have several important certificates. The production quality management system is certified according to ISO 9001 by the certification body “GLOBAL-CERTIFIC.” In addition, our products meet European TÜV NORD standards, confirming their high quality and compliance with international standards. We also have a Certificate of Conformity from Deutsche Bahn, which is a significant indicator of the reliability and quality of our products. Our G4Si1 wire has successfully passed testing at the E.O. Paton Electric Welding Institute and can be used in the production and installation of steel bridge structures. DNIPROMETYZ TAS has also been granted the right to mark its products with the CE mark, indicating compliance with safety and health requirements in the European Union.

## LOOKING TO THE FUTURE

In the future, we plan to continue investing in the latest technologies and expanding our product range to meet our customers’ needs. We are confident that the use of our high-efficiency welding wire will help our customers adapt to new challenges and succeed in their activities.

Our vision for the future is to create innovative solutions that will enable welding technologies to reach new heights, ensuring high quality, reliability, and environmental friendliness.

DNIPROMETYZ TAS is always ready to support its customers on the path to success by providing them with the best products and solutions in the welding materials market.